

**Axial Behavior and Transverse Reinforcement Requirements of UHPC  
Columns with Emerging Mixtures: Assessment of Existing ACI Provisions  
and New Developments**

Final Report Submitted to:  
ACI Foundation Concrete Research Council

By:  
Milana Cimesa  
Allan J. Romero  
Mohamed A. Moustafa



University of Nevada, Reno  
Department of Civil and Environmental Engineering

July 2023

## ABSTRACT

Advanced materials, such as ultra-high performance concrete (UHPC), are among the emerging technologies that can revolutionize our future structures with significantly improved strength and durability for a much longer service life than conventional concrete. Behind the excellent performance of UHPC stands its dense packing theory which excludes the usage of coarse aggregates and incorporates steel fibers to bridge the microcracks and provide high post-cracking strength and ductility. Emerging UHPC mixtures may also contain carbon nanofibers (CNFs) that further enhance the nanostructure of UHPC and its cracking behavior. Furthermore, to lower the high cost of the UHPC, economic semi-proprietary mixtures can combine with proprietary dry blends with locally available sand and cement, and could be further optimized for cost by using recycled steel fibers. Most traditional or emerging UHPC mixtures, such as the CNF-enhanced or semi-proprietary mixtures, applications are for bridge field joints and overlays among other small-scale applications. Exploring the behavior and the design of robust traditional, CNF-enhanced, and semi-proprietary UHPC mixtures when used in full structural components will provide the understanding and the tools to expand the use of UHPC in large structural applications or full systems. Due to the lack of a comprehensive database on full-scale UHPC columns, this research study provides a careful look at the axial behavior of UHPC columns in the context of varying UHPC mixtures and transverse reinforcement detailing effects. Thus, this study explores the structural behavior and deformation capacity of 13 full-scale UHPC square and rectangular columns tested at the 4,000-kip (17,800 kN) machine at the University of California, Berkeley under axial loading. In addition, data from seven more full-scale columns are used in order to calibrate and finalize the axial load design equation for UHPC columns. The report discussion is concerned mainly with presenting and interpreting the axial behavior of the columns made of the traditional, CNF-enhanced, and semi-proprietary UHPC mixtures, but with a particular focus on the effects of ACI- and non-ACI compliant transverse reinforcement detailing square and rectangular full-scale columns.

## **ACKNOWLEDGEMENT**

The study presented in this report is funded by the Concrete Research Council (CRC) of the American Concrete Institute Foundation (ACIF) through a 2021 research grant. All materials were generously provided by our industry partners for this project: Steelike, ceEntek, and Cor-Tuf, whose support and in-kind donation are greatly appreciated.

Disclaimer: All results and conclusions presented herein are those of the authors and do not necessarily represent the sponsors' and industry partners' views.

## TABLE OF CONTENTS

ABSTRACT .....	i
ACKNOWLEDGEMENT .....	ii
TABLE OF CONTENTS.....	iii
LIST OF TABLES.....	vi
LIST OF FIGURES .....	vii
1 Introduction.....	1
1.1 Overview and Literature Review .....	1
1.2 Problem Statement .....	4
1.3 Research Objectives.....	5
1.4 Methodology .....	6
1.5 Report Outline .....	6
2 Experimental Program Development.....	7
2.1 UHPC Mixtures and Columns Groups.....	7
2.1.1 UHPC Type A.....	7
2.1.2 UHPC Type B.....	9
2.1.3 UHPC Type C.....	10
2.2 Materials Testing Setup.....	12
2.3 Columns Fabrication .....	13
2.4 Test Matrix .....	15
2.5 Reinforcement Configuration.....	17
2.6 Columns Test Setup and Instrumentation .....	19
3 Material Tests Results and Modulus of Elasticity .....	22
3.1 Data Processing and Interpretation .....	22

3.2	Results from Type A Cylinders.....	22
3.3	Results from Type B Cylinders.....	24
3.4	Results from Type C Cylinders.....	24
4	Axial Behavior of Columns .....	27
4.1	Type A Columns .....	27
4.1.1	Summary of Key Results .....	28
4.1.2	Damage Progression .....	29
4.1.3	Force versus Deformation Relationships .....	30
4.1.4	Force versus Axial Strain Relationships .....	30
4.1.5	Longitudinal and Transverse Reinforcement Strains.....	33
4.2	Type B Columns.....	35
4.2.1	Summary of Key Test Results .....	35
4.2.2	Construction Challenges .....	36
4.2.3	Damage Progression .....	38
4.2.4	Force versus Deformation Relationships .....	39
4.2.5	Force versus Axial Strain Relationships.....	40
4.2.6	Longitudinal and Transverse Reinforcement Strains.....	41
4.2.7	Concrete Surface Strain .....	44
4.3	Type C Columns.....	45
4.3.1	Summary of Key Results .....	45
4.3.2	Damage Progression .....	46
4.3.3	Force versus Deformation Relationships .....	47
4.3.4	Force versus Axial Strain Relationships.....	47
4.3.5	Longitudinal and Transverse Reinforcement Strains.....	50

5	Axial Load Design and Detailing .....	54
5.1	Calculation of Axial Load Capacity Reduction Factor .....	54
5.2	Effect of Transverse Reinforcement Detailing.....	56
6	Concluding Remarks.....	58
6.1	Summary .....	58
6.2	Key Observations and Conclusions.....	58
6.3	Design Recommendations.....	60
	REFERENCES .....	62

## LIST OF TABLES

<b>Table 2-1</b> Mix ingredients and proportions of UHPC Types A, B, and C in lb/ft <sup>3</sup> (kg/m <sup>3</sup> ).....	8
<b>Table 2-2</b> Test matrix identifying varied fiber reinforcement, UHPC mixture types, and both longitudinal and transverse reinforcement configurations.....	16
<b>Table 2-3</b> Additional columns used in Chapter 5 for the axial load design equation assessment	17
<b>Table 2-4</b> Tensile properties of different reinforcing steel bar sizes used int this study.....	18
<b>Table 3-1</b> Summary of compression strength and modulus of elasticity values using three different stress-strain regions for Type A cylinders at different ages .....	23
<b>Table 3-2</b> Summary of compression strength and modulus of elasticity values using three different stress-strain regions for Type B cylinders at different ages.....	24
<b>Table 3-3</b> Summary of compression strength and modulus of elasticity values using three different stress-strain regions for Type C cylinders at different ages.....	25
<b>Table 4-1</b> Summary of key test results of Type A UHPC columns .....	28
<b>Table 4-2</b> Load values at onset of yielding strain of the longitudinal bars in Type A columns ..	35
<b>Table 4-3</b> Summary of key test results of all four Type B columns .....	36
<b>Table 4-4</b> The yielding strain of the longitudinal bars in Type B columns .....	43
<b>Table 4-5</b> Summary of key test results of all five Type C columns.....	45
<b>Table 4-6</b> The yielding strain of the longitudinal bars in Type C columns .....	53
<b>Table 5-1</b> Axial load design reduction ( $\alpha$ ) factor estimation using ACI-compliant columns .....	56
<b>Table 5-2</b> Design and actual axial capacity of UHPC columns with varying transverse reinforcement detailing and ACI compliance .....	57

## LIST OF FIGURES

<b>Figure 2.1</b> (a) UHPC Type A ingredients; (b) illustration of adding the steel fibers into the mixture; and (c) photograph of sample cast UHPC Type A columns (horizontally positioned) .....	8
<b>Figure 2.2</b> (a) UHPC Type B ingredients including the CNF paste; (b) illustration of adding the thick CNF paste into mixture; and (c) photograph of fresh UHPC Type B casting of a column. 10	
<b>Figure 2.3</b> Overview of all dry and fluid ingredients of UHPC Type C.....	11
<b>Figure 2.4</b> Visual comparison of samples from manufactured steel fibers and recycled tire fibers .....	11
<b>Figure 2.5</b> Compression tests: (a) final prepared specimens after grinding; (b) typical instrumentation with three LVDTs placed to capture axial shortening; and (c) typical test setup	13
<b>Figure 2.6</b> (a) Rebar cages and close up view of an instrumented transverse rebar; (b) formwork and typical installed rebar cage; (c) UHPC mixing equipment and set up; (d) view of the different fabricated columns at UNR fabrication yard; (e) loading the columns on flatbed truck to be transported to the PEER Laboratory for testing; and (f) stacked columns after delivery in CA ..	14
<b>Figure 2.7</b> Reinforcement details in elevation views and cross-sections for different columns..	18
<b>Figure 2.8</b> Schematic drawing of the PEER UTM and typical test setup and instrumentation ...	19
<b>Figure 2.9</b> Actual photographs of: (a) the 4,000-kip PEER UTM and load frame; (b) forklift handling of one of the columns using the #8 lifting bars; (c) location of the LVDTs at one of the columns sides; and (d) dimensions of the gage lengths captured by LVDTs and string pots .....	20
<b>Figure 3.1</b> Stress-strain curves of Type A UHPC at: (a) 28-days age, and (b) test day .....	23
<b>Figure 3.2</b> Compressive stress-strain curves of Type B UHPC captured at: (a) 28 days, (b) 105 days, and (c) test day.....	26
<b>Figure 3.3</b> Compressive stress-strain curves of Type C UHPC captured at 28 days (left) and test day (right).....	26
<b>Figure 4.1</b> Mode of failure of the four different Type A columns after testing.....	29
<b>Figure 4.2</b> Force versus deformation relationships for Type A columns using the three different LVDTs or SP sets.....	31

<b>Figure 4.3</b> Force versus axial strain for all four Type A UHPC columns as obtained from different measurement sets along with comparison of the overall average curves of all columns .....	32
<b>Figure 4.4</b> Force versus longitudinal rebars strain at different locations and heights along height in all four Type A columns .....	33
<b>Figure 4.5</b> Force versus selected transverse rebars strain at different locations and heights along height in all four Type A columns .....	34
<b>Figure 4.6</b> Honeycombs and delamination of Type B columns.....	37
<b>Figure 4.7</b> Photographs of the Type B UHPC columns failure after axial testing.....	38
<b>Figure 4.8</b> Average force versus deformation relationships for all Type B columns using different LVDTs and SP measurement sets.....	39
<b>Figure 4.9</b> Force versus axial strain for all four CNF-enhanced Type B UHPC columns.....	40
<b>Figure 4.10</b> Force versus strain in corner longitudinal bars in Type B rectangular columns .....	41
<b>Figure 4.11</b> Force versus strain in middle longitudinal bars in Type B rectangular columns .....	42
<b>Figure 4.12</b> Force versus strain of the transverse bars in columns .....	43
<b>Figure 4.13</b> a) concrete gages installed on the top and bottom of the column, b) load versus strain in concrete captured by transverse and longitudinal concrete gages, c) comparison of the average concrete strain captured by longitudinal and lateral concrete gages with the overall axial strain of the column.....	44
<b>Figure 4.14</b> Mode of failure and damage pictures of the five tested Type C columns .....	46
<b>Figure 4.15</b> Average force versus deformation relationships for all Type C columns using different BR, SR, and SP measurement sets.....	48
<b>Figure 4.16</b> Force versus axial strain for all five Type C columns and comparisons of overall average curves for five columns together .....	49
<b>Figure 4.17</b> Force versus strain of the middle longitudinal bars in selected Type C columns .....	50
<b>Figure 4.18</b> Force versus strain of the corner longitudinal bars in all Type C columns .....	51
<b>Figure 4.19</b> Force versus strain of the transverse reinforcement at different levels along the height in the five Type C columns.....	52

# 1 INTRODUCTION

## 1.1 Overview and Literature Review

Even though ultra-high performance concrete (UHPC) has major features of mortars, it is widely known and perceived as superior concrete class. Behind the excellent performance of this type of concrete stands its dense packing which excludes the usage of coarse aggregates and incorporates steel fibers in order to bridge the microcracks and provide high post-cracking tensile strength with the increase of ductility, avoiding the brittleness of the concrete (Abokifa and Moustafa 2022). The compressive strength of UHPC can be four to six times higher, while tensile strength is approximately two times higher, when compared to normal strength concrete (NSC). Although all these features are promising to be used in diverse applications, this type of concrete is mainly used in bridge construction, primarily for relatively small applications such as field joints and deck overlays, and to less extent in structural elements like link slabs or full girders. The reason for the less common large scale applications is the high material cost, lack of comprehensive knowledge and contractors expertise on the process of the mixing, and absence of design guidance applicable for this type of material (Graybeal, 2014).

As mentioned before, due to the excellent performance of the UHPC, many research studies are investigating the behavior of this type of concrete at different scales. With focus on axial behavior and columns, and at a relatively smaller scale, Naeimi and Moustafa (2021) did the experiments on more than 130 unconfined and confined  $2 \times 4$  in ( $51 \times 102$  mm) and  $3 \times 6$  in ( $75 \times 150$  mm) cylinders under compressive loading. Along with the different cylinders size, other variables were steel fiber ratios (0, 2, and 4%) and spiral transverse ratios (0, 2, 4, and 8%). They concluded that spiral reinforcement helped increase strength and ductility, where the enhancement of ductility was more significant. Furthermore, this enhancement was primarily due to the steel spirals' usage compared to the steel fiber's effects. Also, the stress-strain curves for the unconfined specimens had a linear behavior up to the peak point, followed by a sudden drop. In contrast, the stress-strain curves of confined specimens could be separated into three regions: linear, nonlinear hardening, and post-peak softening. The observations and conclusions on confinement behavior of UHPC cylinders motivated the researchers at the University of Nevada, Reno (UNR) to explore full columns in several projects, including this study herein, as mentioned later.

Furthermore, some research studies are investigating the behavior of UHPC for various applications and exploring new technologies. For example, a recent study by the authors (Cimesa and Moustafa 2022) investigated the behavior of carbon nanofiber (CNF)-enhanced UHPC cylinders under compressive loading. More than 230 unconfined and confined  $3 \times 6$  in ( $75 \times 150$  mm) cylinders were tested. The variables in that experimental campaign included transverse reinforcement ratios (0, 2, and 4%) and steel fiber ratios (0-4%) at a constant CNF ratio throughout the batches (0.5% by volume). The study fully characterized the CNF-enhanced UHPC compressive stress-strain relationship and modulus of elasticity at different ages. Furthermore, the study showed that CNF could further enhance the post-peak ductile behavior in cylinders confined adequately by transverse reinforcement and steel fibers. Cimesa and Moustafa (2022) also found that analytical models proposed by Naeimi and Moustafa (2021) for conventional UHPC do not precisely predict the post-peak behavior of this novel type of UHPC.

Even though UHPC has excellent mechanical properties, this type of concrete is usually associated with a high cost. The development of non-proprietary and semi-proprietary UHPCs is currently being explored as a viable solution to reduce the costs associated with UHPC materials, transportation, and production by leveraging domestic and local materials. The Federal Highway Administration (FHWA) along with various research teams have developed design guidelines for non-proprietary UHPC in bridge applications (e.g. Graybeal, 2013; Berry et al. 2017; El-Tawil et al. 2016). Moreover, an independent research study by Abokifa and Moustafa (2021a, 2021b) investigated the application of non-proprietary UHPC with different aggregate gradations for accelerated bridge construction (ABC) field joints. They tested two full-scale specimens of deck bulb tee girders (DBT) top flange sections with longitudinal field joints, exposing them to static vertical loading using commercially available and non-proprietary UHPC mixtures. Abokifa and Moustafa (2021a) concluded that the non-proprietary UHPC mixture composed of local ingredients from Nevada and California provided satisfying mechanical properties and met all specified performance specifications for ABC applications. Furthermore, the work on non-proprietary UHPC by Abokifa and Moustafa (2021a) was extended to compare the structural behavior of bridge deck subassembly specimen with non-proprietary UHPC closure pours to that of similar specimen with robust commercially available UHPC to provide ultimate validation for the proposed non-proprietary mixtures.

Steel fibers, a crucial constituent of UHPC, are a primary reason for the high price. A proposed solution to reduce the cost of fiber-reinforced concrete is replacing steel fibers with recycled steel fibers that can be extracted from recycled tires and wires for instance. One popular source for recycled tires fibers are those derived from scrap car tires in city landfills, typically piled for burning. However, these landfill tires can be processed to remove the wire fibers through different recycling methods, such as pyrolysis, shredding, and mechanical recycling (Liew and Akbar 2020). With recycled fiber's success and promising results in NSC, applying these recycled fibers has opened possibilities for a more cost-effective, greener, and more sustainable UHPC. Limited studies have been conducted in the past few years investigating the effect of recycled fibers in UHPC. Abdolpour et al. (2021) performed a mechanical characterization of recycled fibers in UHPC. The study conducted compressive and tensile tests, and the results showed a 4% decrease in compressive strength while an improvement in tensile ductility for a fiber ratio greater than 1%. Moreover, Yang et al. (2019) compared UHPC with two types of recycled and three industrial steel fibers. The study showed that all types of fibers exhibited excellent mechanical properties; however, fibers with rubbers' presence have relatively decreased compressive and tensile strength. Overall, the emergence of new studies incorporating recycled fibers in UHPC has been promising in the past years. Nevertheless, these studies have been mainly limited to small applications, and no research has been conducted yet to utilize recycled fibers in large-scale structures.

While a significant amount of work was done on small-scale compressive UHPC specimens, a relatively small body of literature investigates the axial behavior of structural elements made entirely out of UHPC confined with traditional reinforcement. One of those recent studies was funded by the ACIF, similar to the one in hand, and focused on slender columns and different reinforcement detailing (Aboukifa and Moustafa 2022a; 2022b). In the first part of the study (Aboukifa and Moustafa 2022a), five square full-scale structural columns of 11 ft (3.35 m) height were fabricated using a commercially available UHPC mixture and tested under axial load. The aim was to investigate the reinforcement detailing effects while varying 1 and 2% of the steel fiber ratios to capture the mechanical behavior of the columns under the monotonic compressive loading. This research study has provided a deeper insight into the empirical reduction factor for axial strength design, and proposed a factor of 0.75 for determining the axial capacity of UHPC columns. Furthermore, this study contributed to understanding UHPC columns' failure mode, which turned out to be a sudden failure close to the point of maximum axial capacity by buckling

the longitudinal rebars followed by the transverse reinforcement rapture and spalling of cover concrete. Also, they observed that a reduction of the steel fiber ratio from 2 to 1% would not affect the axial capacity of the column if sufficient transverse reinforcement is provided, but rather have an impact on peak and ultimate strain, which decreased by 16%. Moreover, the effect of steel fibers was interpreted as internal confinement that postponed the yielding of the transverse reinforcement to be close to reaching the axial capacity of the column. The second part of the work by Aboukifa and Moustafa (2022b), five UHPC columns with different slenderness ratios were tested and careful recommendations for adopting the ACI 318 Moment Magnification Method for slender UHPC columns were provided.

In conclusion, there is still a need for more experimental data to explore emerging UHPC types and develop proper design guidelines for larger structural applications. There is insufficient knowledge of proper reinforcement detailing for full structural UHPC columns, applicability of the ACI 318-19 design equations and detailing requirements for UHPC, proper steel fiber percentage, and economic alternative UHPC mixtures. This research study aims at filling some of these knowledge gaps by providing exclusive new experimental data for UHPC columns made with three different mixtures, i.e. CNF-enhanced, traditional, and semi-proprietary UHPC mixtures, and further understand the effects of varying transverse reinforcement detailing. In order to accomplish this goal identified above, 13 nine-foot (2.74 m) tall columns were tested under concentric axial compressive loading. The overall goal of this study is to capture the structural behavior and effects of varying reinforcement detailing of: (1) four square columns made of commercially available traditional UHPC mixture, (2) four CNF-enhanced UHPC rectangular columns, and (3) five columns made out of semi-proprietary UHPC mixture with varying steel fibers ratios and types to include recycled tires for the first time. The study also investigates the columns' axial stiffness and strain capacity, and is concluded by proposing a well-calibrated axial design equation using data from the 13 columns of this study along with seven additional UHPC full-scale columns that were recently tested through other projects by the authors.

## **1.2 Problem Statement**

The use of UHPC is expanding worldwide, from bridge deck joints and connections to full components and larger applications. In the United States, several major efforts that include two recent national initiatives were conducted to expand the use of UHPC for structural components.

The first was led by the FHWA and aimed at developing mega bridge girders (the FHWA is also developing the first-in-nation design guidelines for UHPC applications in bridges). The second initiative was led by the Precast/Prestressed Concrete Institute (PCI) and aimed to develop non-proprietary UHPC mixes for precast/prestressed girders. While such efforts are expected to expand the UHPC market further in the US, there has been less focus on UHPC columns and their applications for precast construction, whether for buildings, parking structures, or bridges. To contribute towards filling such a knowledge gap on columns as summarized in the previous section, the PI has recently completed two of projects through the accelerated bridge construction university transportation center (ABC-UTC) and the ACIF CRC on the behavior of seismic and slender UHPC columns. With promising results and findings, the aim is to extend this work and further assess existing ACI provisions for applicability for UHPC columns in ordinary and special frames, focusing on transverse reinforcement detailing requirements. Thus, this project presented herein has considered several full-scale tests to eliminate scale effects and accurately capture the interaction between transverse reinforcement, different types of fiber reinforcement (including CNF and recycled tire fibers) and proprietary and semi-proprietary UHPC mixtures. The new tests provided in this project will add to the previous work conducted on axial UHPC columns to expand UHPC columns database so that future design guidelines development efforts can build on such data to assess transverse reinforcement detailing and confinement requirements for UHPC columns.

### **1.3 Research Objectives**

As mentioned above, this project aims at providing a better understanding of the transverse reinforcement detailing effects on the structural behavior and ductility of UHPC columns from traditional and emerging UHPC mixtures. To achieve this goal, several specific research objectives are defined as follows:

1. Conduct 13 large-scale UHPC column tests with various transverse reinforcement configurations, confinement ratios, steel fiber ratios and types, and varying UHPC mixtures to determine the mechanical properties as they relate to transverse reinforcement details;
2. Assess current ACI 318 columns transverse reinforcement and detailing requirements if applicable or necessary for UHPC columns;

3. Provide design guidance for axial UHPC columns, which can be incorporated into the ongoing effort of ACI Subcommittee 239-C on developing a guide document for the structural design of UHPC.

#### **1.4 Methodology**

This research study is heavily experimental, where 13 nine-foot tall columns are tested under uniaxial compressive loading with more than 135 complimentary cylinders to properly characterize the UHPC used in the columns and capture the strength development over time. The structural behavior of the 13 columns is discussed in full details in Chapter 4 of this report. However, data from seven more additional columns, that were recently tested by the authors as part of other projects, are used along with the 13 columns in this study to ultimately calibrate the axial load design equation as summarized in Chapter 5 of this report. The experimental study incorporates multiscale testing of the specimens containing three types of reinforcement at the nano level, i.e. CNF for the columns made out of ceEntek UHPC mix, micro level (using manufactured and recycled steel fibers), and macro level using traditional transverse reinforcement. Careful instrumentation using several linear variable differential transformers (LVDTs) and wire/string potentiometers were used to capture axial shortening at both material and structural levels when cylinders and columns were tested. Furthermore, strain gages were installed on the rebars' to capture the compressive and tensile strain in the longitudinal and transverse reinforcement of the columns during the loading. Also, surface concrete gages were installed on selected columns to capture local strains and compare them with the global column's behavior captured by LVDTs and string pots.

#### **1.5 Report Outline**

This report is organized into six chapters. Chapter 1 provides an overview of the research topic and brief overview of the relevant literature. The experimental program is discussed in Chapter 2 with focus on construction, materials, test setup and instrumentation. Chapter 3 presents the material characterization of all three types of UHPC mixtures. Chapter 4 provides the structural behavior discussed of the 13 tested columns. Chapter 5 is brief and focus only on the axial load design equation for UHPC columns, and Chapter 6 provides final concluding remarks and design recommendations and guidance for future implementation in design codes.

## 2 EXPERIMENTAL PROGRAM DEVELOPMENT

This chapter presents the experimental testing program of UHPC columns subjected to concentrically monotonic axial loading. In total, results from up to 20 full-scale UHPC columns are included in the final design recommendations. However, the structural behavior of only 13 columns that comprise the core of this study are presented and discussed in full details in Chapter 4. The additional seven columns used in Chapter 5 are from other projects and aim at expanding the data set used in calibrating the axial load design equation. All columns were tested at one of the US's largest axial load testing facilities; the 4,000-kip [17,793 kN] testing machine at the University of California, Berkeley Pacific Earthquake Engineering Research Center (PEER) Laboratory. The experimental program presented herein is discussed in terms of the material properties used to construct the specimens, test setup and testing procedure at both the material and structural levels, test matrix, specimens details and reinforcement configuration, and the instrumentation plan used to capture the columns deformations and strain in rebars.

### 2.1 UHPC Mixtures and Columns Groups

Three different UHPC mixtures were used in the construction of the 13 (+ additional 7) columns used in this study: (1) Steellike UHPC, which is referred to as Type A in this report; (2) CeEntek CNF-enhanced UHPC, which is referred to as Type B, and (3) Cor-Tuf UHPC, which is referred to as Type C. Accordingly, the 13 columns discussed in details in this report are categorized into three groups.

#### 2.1.1 UHPC Type A

The first group of columns used Type A UHPC and consists of four square columns with cross-section dimensions of  $12 \times 12$  in ( $30.5 \times 30.5$  cm). This group represents the first UHPC mixture that in turn, represents traditional UHPC from Steellike. The Steellike UHPC mixture uses white cement, which gives a unique bright or white appearance when the concrete sets, as shown in Figure 2.1. According to Hamad (1995), white cement is a Portland cement made following the ASTM C150 specification suitable for Type I and III cement. The research study by Moresove and Skvara (2001) agrees with Hamad (1995) that the white color of this cement comes from a different manufacturing process when compared to the process of making gray cement. White cement is made out of carefully selected raw materials with a negligible amount of iron oxide

and magnesium oxide that are responsible for the gray color of traditional Portland cement. When gray and white types of cement are compared, the research study by Hamad (1995) concluded that white cement has a shorter setting time and can lead to higher ultimate compressive and tensile strength. Besides the dry mix of the Steelike UHPC, which is consisted of white cement, fine sand, and pozzolanic materials, this type of UHPC contains water, steel fibers, and admixtures, as presented in Figure 2.1. Table 1-1 provides the mix proportion suggested by Steelike containing 2% steel fiber by volume, which is again labeled as Type A mixture thereafter.



**Figure 2.1** (a) UHPC Type A ingredients; (b) illustration of adding the steel fibers into the mixture; and (c) photograph of sample cast UHPC Type A columns (horizontally positioned)

**Table 2-1** Mix ingredients and proportions of UHPC Types A, B, and C in lb/ft<sup>3</sup> (kg/m<sup>3</sup>)

UHPC Mix	Fibers (%)	Mix Ingredients in lb/ft <sup>3</sup> (kg/m <sup>3</sup> )						
		Steel Fibers	Recycled Tire Fibers	Premix	Water	Ice	CNF paste	Admixture
Type A	2%	9.8 (157.0)	-	133.5 (2138.5)	74.0 (118.5)	4.9 (79.0)	-	0.6 (9.8)
Type B	2%	9.7 (156.0)	-	143.6 (2300.0)	10.1 (161.0)	-	0.8 (13.2)	1.4 (23.0)
Type C	1%	4.9 (78.6)	-	137.0 (2194.5)	10.0 (160.2)	-	-	5.0 (77.5)
Type C	2%	9.8 (157.2)	-	137.0 (2194.5)	10.0 (160.2)	-	-	5.0 (77.5)
Type C	2%	-	9.8 (157.2)	137.0 (2194.5)	10.0 (160.2)	-	-	5.0 (77.5)

In general, the mixing of UHPC Type A ingredients lasted about 13 minutes. For the construction of the columns and material sampling in this study, the dry mix was first added slowly into an Imer Mortman 360 high-shear mixer. After one minute of mixing, the water, that was previously mixed with the admixtures, was slowly added to the dry mixture. The Type A columns construction took place early Fall of 2021 in Reno, NV. Due to the high temperatures during the day that exceeded

75 °F (24 °C), ice was added immediately following the dry powder, water, and admixtures and such blend was mixed for about 10 minutes. When the right consistency was achieved, steel fibers were added, as illustrated in Figure 2.1, and mixed with the rest of the ingredients for another one or two minutes only to avoid segregation of the steel fibers on the bottom of the mixer. When the mixing was done, the concrete was poured into the columns' formwork positioned horizontally, as also shown in Figure 2.1. More details about the columns and construction are provided later.

### *2.1.2 UHPC Type B*

The second group of columns used UHPC Type B and consisted of four rectangular columns with cross-section dimensions 10 × 16 in (25.4 × 40.6 cm). Group B columns were fabricated using a commercial UHPC mixture containing CNF and provided by ceEntek; the CNF-enhanced UHPC is labeled as Type B UHPC mixture herein. The unique component of this type of UHPC is a thick black-colored paste containing dispersed carbon nanofibers (of about 0.5% by volume) mixed with admixtures. The different components of UHPC Type B and illustration of the carbon nanofiber paste are shown in Figure 2.2. According to the vendor's specifications, the CNF volumetric ratio was not possible to change within the black paste, and as such, 0.5% by volume CNF was used for all material trial and columns fabrication batches. In general, the CNFs fill the nanopores, preventing nano cracks from propagating into the micro-cracks (Yoo et al. 2022). Besides the cracking resistance, CNF can enhance the fracture toughness of this class of UHPC materials (Meng and Khayat 2018). According to Meng and Khayat (2018), when the amount of CNF is increased from 0 to 0.3% and incorporated into the UHPC mixture, the porosity is reduced by 35%, capillary pores by 75%, and gel pores are increased by 70%. Also, with the properly selected admixtures, CNF help with enhancing the bond between steel fibers and the cement paste (Sbia et al. 2014). Besides the CNF paste from CeEntek, the main other ingredients of this UHPC mixture are water, 2% of steel fibers, calcium nitrate accelerator (70% liquid), and a preblended prebagged dry mixture consisting of fine sand, pozzolanic material, and cement as shown in Figure 2.2. Table 1-1 above presents the mixing proportions as provided by the vendor's specifications.

The procedure of mixing UHPC recommended by ceEntek was similar to the mixing of Steellike. The only difference was the time of the mixing, which was almost two times longer when compared to Type A due to few reasons such as: (1) the higher percentage of accelerator used, relative to water and other fluids, which generated more internal heat during mixing and lowered

the workability; (2) the addition of CNF paste required more time, and (3) the low temperature in Reno during the mixing of all UHPC Type B batches that extended into winter of 2021. It is worth noting when temperatures are low, there is no need to use ice for replacing any portions of the water, and as such, mixing time can in general get little longer in the absence of ice.

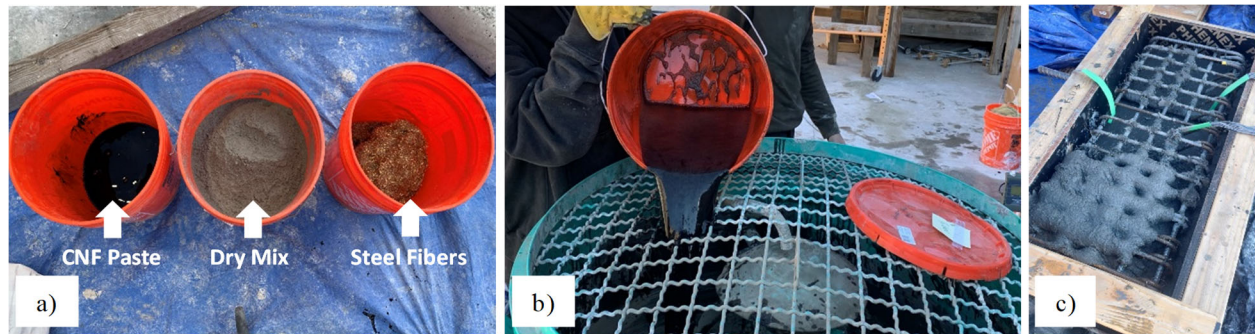


**Figure 2.2** (a) UHPC Type B ingredients including the CNF paste; (b) illustration of adding the thick CNF paste into mixture; and (c) photograph of fresh UHPC Type B casting of a column

### 2.1.3 UHPC Type C

The last group of columns, i.e. Group C, consisted of five square columns with  $12 \times 12$  in ( $30.5 \times 30.5$  cm) in cross-section dimensions, which are similar to Group A columns dimensions. This last group of columns was made out of the Cor-Tuf UHPC, which is labeled here as Type C. The authors choose to also refer to this specific type of UHPC in this report as a semi-proprietary UHPC because of the use of locally available sand, cement, and admixtures along with a proprietary preblended prepackaged dry mix (CT powder). The semi-proprietary nature stems from the fact that it is up to the customer, or our research team in this case, to source and specify sand, cement, and admixtures within general guidance from the vendor. Besides the dry mix, which is consisted of locally available sand and cement, Cor-Tuf preblended constituent (i.e. CT powder) is primarily composed of quartz and silica fume. In this study, we used this type of semi-proprietary UHPC with both manufactured virgin steel fibers and recycled tires fibers. All ingredients were mixed with water and three types of admixtures as shown in Figure 2.3. Again, Table 1-1 presents the mix proportion used for the fabrication of Group 3 columns that varied the steel fibers to include 1% and 2% of virgin steel fibers and 2% of recycled fibers.

Because the recycled fibers have varying densities due to different fiber aspect ratios and impurities as illustrated in Figure 2.4, the amount of the recycled fibers was determined based on

the weight corresponding to the total weight of the steel fibers used in the other columns that contained 2% of steel fibers by volume. The 2% by volume of manufactured steel fibers typically corresponds to about 6% by weight. Using weight comparison instead of density based was deliberately chosen to assess whether the same amount of recycled fibers can perform as an alternative for manufactured fibers.

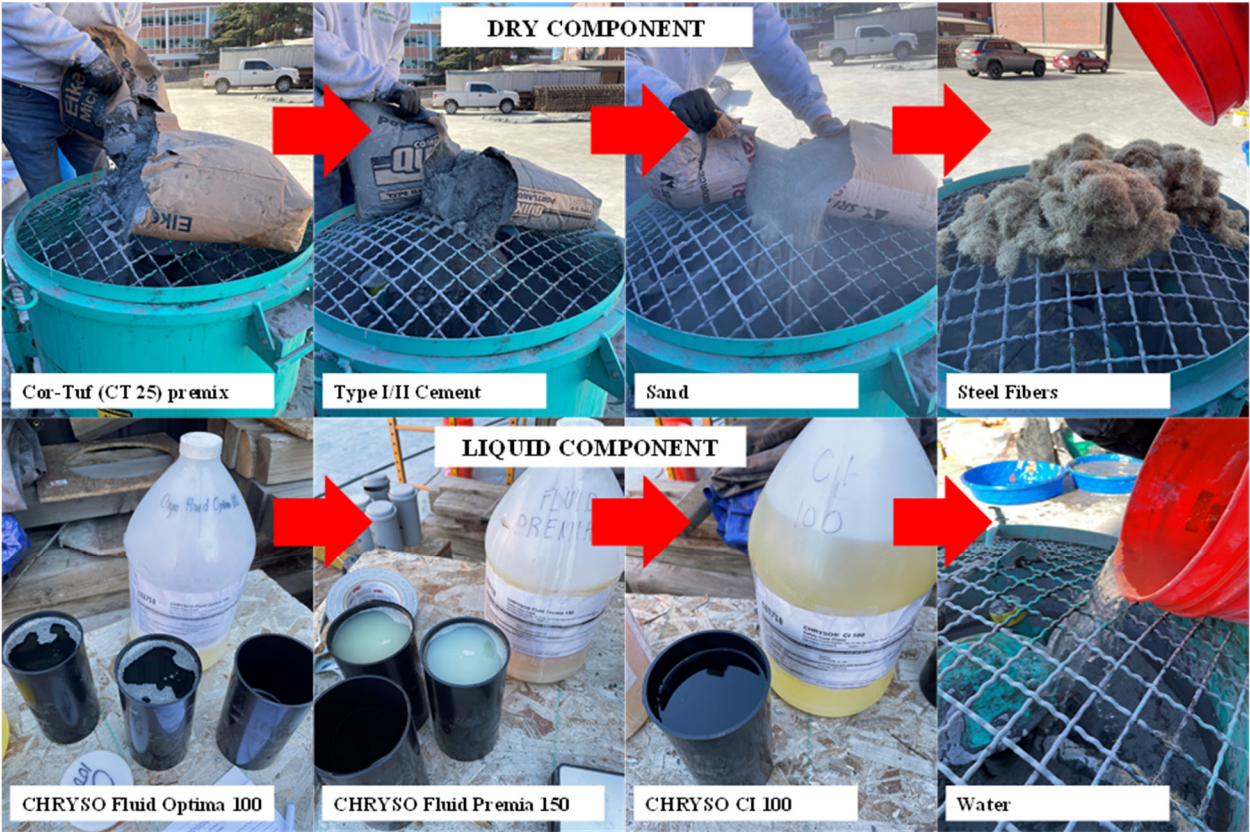


**Figure 2.3** Overview of all dry and fluid ingredients of UHPC Type C



**Figure 2.4** Visual comparison of samples from manufactured steel fibers and recycled tire fibers

It is worth mentioning that the same commercially available steel fibers were used for all columns except for the one column in Group C that incorporated recycled tire fibers. According to the fabricator datasheet, the diameter and length of the manufactured steel fibers are 0.008 and 0.5 in (0.2 and 12.7 mm), respectively, with a yielding stress of 400 ksi (2751 MPa). The visual comparison of the manufactured virgin steel and recycled tire fibers is shown in Figure 2.4.

## **2.2 Materials Testing Setup**

More than 135 cylinders were sampled from the various different material batches used to fabricate the columns and left next to their respective columns to be cured in same conditions as columns. The cylinders were tested to characterize the compressive behavior of UHPC Types A, B, and C in terms of the modulus of elasticity, compressive strength, and full stress-strain relationships. For sampling, the UHPC was placed in  $3 \times 6$  in ( $75 \times 150$  mm) plastic cylinder molds and tapped with a rubber hammer a number of times on the sides to release the entrapped air. All of the cylinders were placed outdoors in the UNR Structures Laboratory fabrication yard, beside columns, to go through the same temperature cycles and better represent the behavior of the columns. It is worth mentioning that none of the cylinders went through a treated regime such as steam curing or a controlled lab environment curing. Therefore, all cylinders went through the natural curing process of the casting environment, which might have included even some freeze-thaw cycles during some of the severe climate days in Reno when this project was taking place.

The compression tests were done according to the methods defined in ASTM C1856 using a compressive SATEC 500 kip (2224 kN) machine under a 0.15 ksi/sec (1.05 MPa/sec) rate of loading. The machine and test setup are shown in Figure 2.5. The rate of loading was determined based on the recommendations by Graybeal (2006) that loading rates between 0.035 ksi/sec and 0.25 ksi/sec (0.24-1.7 MPa/sec) do not have any adverse effects on the compressive behavior of the specimens. A minimum of three specimens were tested at 28 and columns test-days in order to capture the average stress-strain behavior and compressive strength. As required by ASTM C1856, all UHPC cylinders had to be properly prepared. As such, cylinders were first released from the plastic molds, then the top rough surface was cut using a saw-cutting machine. After cutting, both top and bottom surfaces of the specimens were ground using a special dedicated grinding machine to get parallel, smooth, and leveled cylinder ends. Figure 2.5a shows a sample of prepared and ready-to-test UHPC cylinders. Even though the specimens were cut and ground, which caused

their height-to-diameter ratio to be lower than 2, according to Naeimi and Moustafa (2021), a slightly less than 2 height-to-diameter ratio should not adversely affect the specimens' behavior or estimated strength. To capture the axial shortening and, in turn, calculate compression strains, three linear variable differential transformers (LVDTs) were placed around each cylinder with  $120^\circ$  in between, as shown in Figure 2.5. The average deformation derived from all three LVDTs in a typical test was then divided by the average height of the specimen to get the values of the axial strain. Figures 2.5b and 2.5c show an overview of the typical instrumentation and test setup.

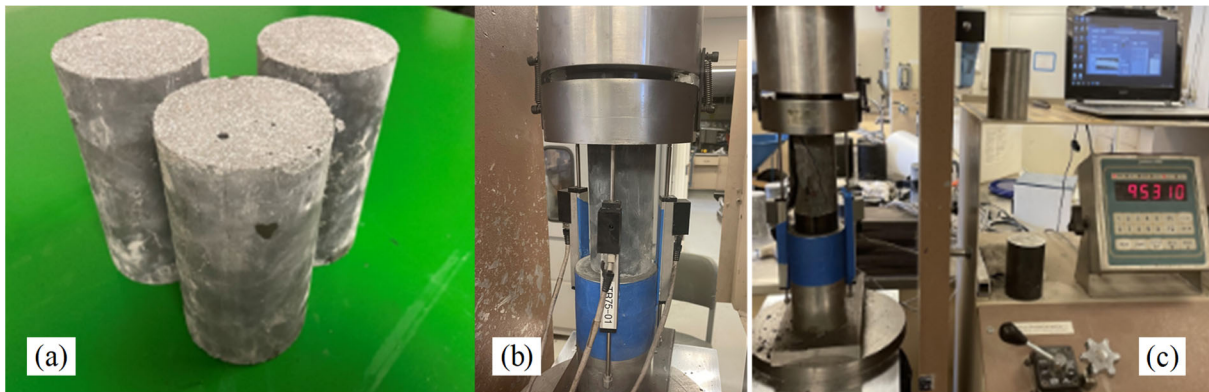


**Figure 2.5** Compression tests: (a) final prepared specimens after grinding; (b) typical instrumentation with three LVDTs placed to capture axial shortening; and (c) typical test setup

### 2.3 Columns Fabrication

As mentioned earlier, all columns used in this study were cast at the UNR Structures Laboratory fabrication yard that can be seen in some of the photographs in Figure 2.6. The columns fabrication went through various stages. First, all the rebar cages for the different columns that had different reinforcement detailing, as explained in the next section, were tied and assembled at a fabricator workshop then delivered to UNR fabrication yard as shown in Figure 2.6a. While already tied, all rebar cages were carefully instrumented with strain gages on selected longitudinal and transverse reinforcement bars to later capture the compressive and tensile strains at 20 to 30 different locations throughout each column during the testing. Next, wood formwork were fabricated as horizontally laid boxes to the dimensions of the columns as shown in Figure 2.6b. All instrumented rebar cages were then placed into the formwork boxes (Figure 2.6b), strain gages cables were organized and bundled to exit the formwork at carefully selected locations, then mixing and furnishing the different UHPC types for all columns commenced and fabrication was completed over the course of approximately three months.

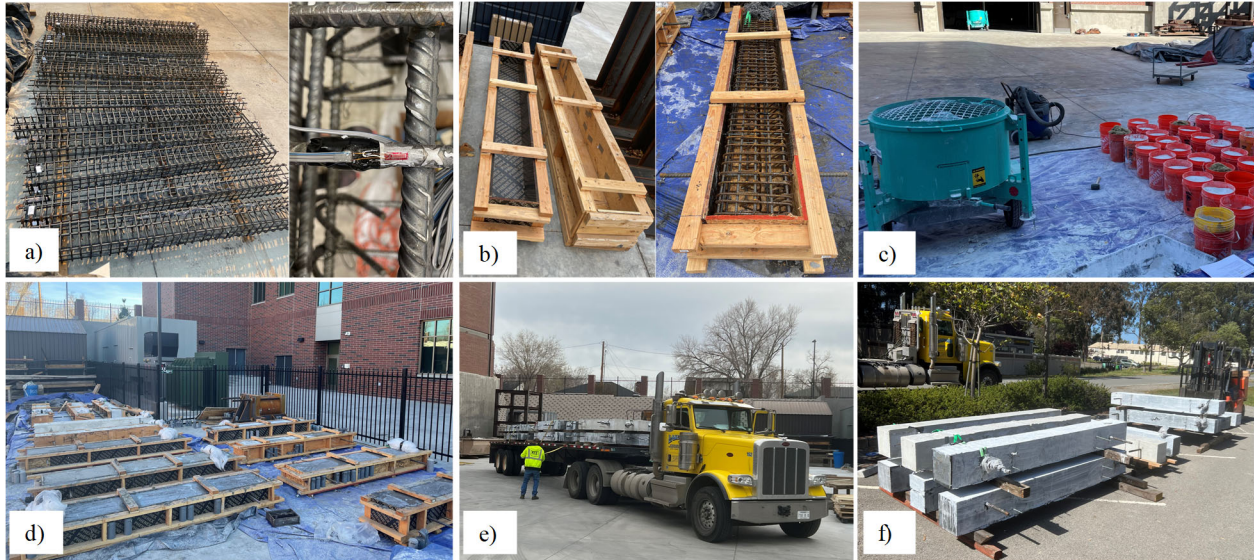


**Figure 2.6** (a) Rebar cages and close up view of an instrumented transverse rebar; (b) formwork and typical installed rebar cage; (c) UHPC mixing equipment and set up; (d) view of the different fabricated columns at UNR fabrication yard; (e) loading the columns on flatbed truck to be transported to the PEER Laboratory for testing; and (f) stacked columns after delivery in CA

The columns were placed horizontally during the pouring of the UHPC as illustrated in Figure 2.6d. In order to capture the progression of the strength over time and on the test-day, which was approximately about seven months after the casting of concrete, at least six cylinders per column were poured and placed alongside the columns to go through the same temperature cycles as the columns. For the CNF-enhanced Type B columns, we faced some challenges and complications during the construction phase. Some columns had significant cold joints, that later led to delamination between the cast layers close to failure when tested, which is discussed more when the final results are presented in Chapter 4. Besides the already low water-to-cement ratio, which can cause an adverse effect on the UHPC mixing (Aboukifa et al. 2021), cold joints and honeycombing may be due to the cold weather and the high percentage of the accelerator used. Due to the low temperatures, some water particles were frozen, preventing proper bonding with the cementitious material. A high dosage of the accelerator substituted a percentage of water that would otherwise be beneficial in terms of enhancing the hydration process and flowability. Consequently, dry mix particles lacked proper hydration bonding to create flowable mass, making cement particles only act as a filler.

In order to try to prevent water evaporation/freezing after the casting day due to the temperature oscillations during the day and freezing temperatures over the night in Reno during the winter time, all columns were covered by heat blankets for approximately two weeks. The heat blankets partially helped prolong the hydration and prevent the freezing of the water particles. After approximately seven months after the casting of the columns, all specimens were transported from UNR Fabrication yard in Reno, NV to the UC Berkeley PEER Laboratory in Richmond, CA as shown in Figures 2.6e and 2.6f.

## **2.4 Test Matrix**

As mentioned above, 13 columns that comprise three groups based on the three different UHPC mixtures, i.e. Types A, B, and C, were fabricated. The columns had varying reinforcement details as explained and summarized in the test matrix in Table 2-2. Overall, this test matrix was designed to investigate the behavior of the UHPC columns under compressive loading in terms of axial strength, compressive strain, and stiffness while having the following variables (1) cross-section (square versus rectangular), (2) amount of steel fiber used (1 versus 2%), (3) comparing the performance of the columns with steel and recycled tier fibers, (4) assess the structural behavior of emerging types of UHPC such as the CNF-enhanced and semi-proprietary UHPC columns, and (5) transverse reinforcement detailing (variation in spacing, the diameter of the rebars, and configuration). As mentioned earlier, nine of the 13 columns had square cross-section dimensions  $12 \times 12$  in ( $300 \times 300$  mm) with a height of 9 ft (2.74 m); four of which were fabricated using UHPC Type A while five were fabricated using UHPC Type C. The other remaining four columns were also 9 ft (2.74 m) in height but with rectangular cross-section dimensions  $10 \times 16$  in ( $254 \times 406$  mm) and made out of UHPC Type B. It is worth noting that all columns used in this study are categorized as non-slender columns according to the ACI 318-19 provision.

From Table 2-2, it is noted that transverse and longitudinal reinforcement varied among the columns and more schematic details are presented next in the reinforcement configuration section. The current ACI code and design standards do not yet provide guidelines for UHPC design, and design codes meant for NSC are not necessarily appropriate for UHPC. For example, ACI 318-19 can overestimate the axial load capacity of the columns (Cai et al. 2021). Also, for the seismic columns, using the ACI 318 equations would require more than 10% of transverse reinforcement ratio for UHPC columns with high strength values, which is not feasible and confirms that such

equations are not suitable for UHPC. In this research study, the test matrix considered ACI compliant reinforcement detailing when no unsupported longitudinal rebar with lateral tie spacing exceeded 6 in (150 mm). Also, the longitudinal spacing of the transverse reinforcement, in what we considered ACI-compliant columns, was limited to 3 in (76.2 mm) to avoid buckling between two hoops. For the sake of the discussion in this study, the column that contained only 1% steel fibers or 2% recycled tire fibers were considered non-ACI compliant columns for results categorization and assessment purposes as explained more in Chapter 5. Accordingly, the test matrix included seven ACI-compliant columns: SP-A-1, SP-A-2, SP-B-2, SP-B-4, SP-C-1, SP-C-2, and SP-C-3, and six non-compliant columns: SP-A-3, SP-A-4, SP-B-1, SP-B-3, SP-C-4, and SP-C-5.

**Table 2-2** Test matrix identifying varied fiber reinforcement, UHPC mixture types, and both longitudinal and transverse reinforcement configurations

Column ID	Cross-Section	UHPC Mixture	Steel Fibers Ratio & Type	CNF [%]	Longitudinal Reinforcement	Transverse Reinforcement
SP-A-1	square	Type A	2% virgin	-	8 #5 (ø16)	#3 at 3 in (ø10 at 76.2 mm)
SP-A-2	square	Type A	2% virgin	-	8 #5 (ø16)	#4 at 3 in (ø13 at 76.2 mm)
SP-A-3	square	Type A	2% virgin	-	8 #5 (ø16)	#4 at 6 in (ø13 at 152.4 mm)
SP-A-4	square	Type A	2% virgin	-	8 #5 (ø16)	#3 at 6 in (ø10 at 152.4 mm)
SP-B-1	rectangular	Type B	2% virgin	0.5	12 #4 (ø13)	#3 at 5 in (ø10 at 127 mm)
SP-B-2	rectangular	Type B	2% virgin	0.5	12 #4 (ø13)	#3 at 2.5 in (ø10 at 63.5 mm) w/ internal hoop & crosstie
SP-B-3	rectangular	Type B	2% virgin	0.5	12 #4 (ø13)	#3 at 2.5 in (ø10 at 63.5 mm)
SP-B-4	rectangular	Type B	2% virgin	0.5	12 #4 (ø13)	#3 at 2.5 in (ø10 at 63.5 mm) w/ one crosstie
SP-C-1	square	Type C	2% virgin	-	8 #5 (ø16)	#3 at 3 in (ø10 at 76.2 mm)
SP-C-2	square	Type C	2% virgin	-	12 #4 (ø13)	#3 at 3 in (ø10 at 76.2 mm)
SP-C-3	square	Type C	2% virgin	-	12 #4 (ø13)	#3 at 3 in (ø10 at 76.2 mm) w/ #3 (ø10) octagon hoop
SP-C-4	square	Type C	1% virgin	-	12 #4 (ø13)	#3 at 3 in (ø10 at 76.2 mm) w/ #3 (ø10) octagon hoop
SP-C-5	square	Type C	2% recycled	-	12 #4 (ø13)	#3 at 3 in (ø10 at 76.2 mm)

In addition to the 13 columns presented in Table 2-2, which comprise the core of this study, seven additional columns, from other recent ongoing projects at UNR, are briefly used later in Chapter 5 to complement the discussion on axial load design of UHPC columns. The seven additional

columns were also fabricated from same UHPC Type A (one more column), Type B (two more columns), and Type C (four more columns) and their details are summarized in Table 2-3. The additional Type A and B columns used similar square cross-section with targeted dimensions of 12 × 12 in (30.5 × 30.5 cm) as all square main columns in Table 2-2. However, the four new Type C columns used circular cross-sections with a 16 in (40.6 cm) diameter and used varying hoops and spirals transverse reinforcement detailing and were cast at a precast plant in CA. The precast circular columns are part of a major ongoing research effort that include a total of 12 UHPC bridge columns; four of which are axial columns and eight are seismic columns with varying column-to-footing connections. The four axial columns were just tested at the PEER Structures lab (similar to all other columns in this study) in May 2024, i.e. during the course of writing the last parts of this report, and preliminary results from such columns are exclusively used in Chapter 5 for ultimate validation of the proposed design equation. It is worth noting, for interested audience, that the remaining eight columns from that precast initiative will be connected to properly designed footings with varying accelerated bridge construction (ABC) seismic connections and tested at UNR Earthquake Engineering Laboratory later in Fall 2023.

**Table 2-3** Additional columns used in Chapter 5 for the axial load design equation assessment

Column ID	Cross-Section	UHPC Mixture	Steel Fibers Ratio & Type	Longitudinal Reinforcement	Transverse Reinforcement
SP-A-5	square	Type A	1% virgin	8 #5 (ø16)	#3 at 3 in (ø10 at 76.2 mm)
SP-B-5	square	Type B	2% virgin	8 #5 (ø16)	#3 at 3 in (ø10 at 76.2 mm)
SP-B-6	square	Type B	2% virgin	8 #5 (ø16)	#3 at 3 in (ø10 at 76.2 mm)
SP-C-6	circular	Type C	2% virgin	12 #4 (ø13)	#3 spirals at 3 in (ø10 at 76.2 mm)
SP-C-7	circular	Type C	2% virgin	12 #4 (ø13)	#3 spirals at 1.5 in (ø10 at 76.2 mm)
SP-C-8	circular	Type C	2% virgin	12 #4 (ø13)	#3 hoops at 3 in (ø10 at 76.2 mm)
SP-C-9	circular	Type C	2% virgin	12 #4 (ø13)	#3 hoops at 1.5 in (ø10 at 76.2 mm)

## 2.5 Reinforcement Configuration

All columns were reinforced using A706 Grade 60 (420) longitudinal and transverse bars. Dedicated tensile tests were performed on #3, #4, and #5 (ø10, ø13, and ø16) rebar coupons to determine the actual tensile behavior of each rebar type/size used in this project. The results from rebar tensile tests are presented in Table 2-4 for completeness. Two configurations were used for the longitudinal reinforcement of the different columns with the square and rectangular cross-

sections: either 8 #5 (ø16) or 12 #4 (ø13) as shown in Figure 2.7. Also, the transverse reinforcement and detailing used in the columns varied significantly (either #3 (ø10) or #4 (ø13) hoops and ties were used) as explained in Table 2-2 and fully illustrated in details in Figure 2.7.

**Table 2-4** Tensile properties of different reinforcing steel bar sizes used in this study

Rebar Size	Rebar Diameter, in (mm)	Rebar Grade, ksi (MPa)	Yield Strength, ksi (MPa)	Ultimate Strength, ksi (MPa)	Ultimate Strain
#3 (ø10)	0.375 (9.5)	60 (420)	73 (505)	103 (711)	0.18
#4 (ø13)	0.500 (12.7)	60 (420)	70 (483)	100 (690)	0.15
#5 (ø16)	0.625 (15.875)	60 (420)	71 (491)	96 (662)	0.18

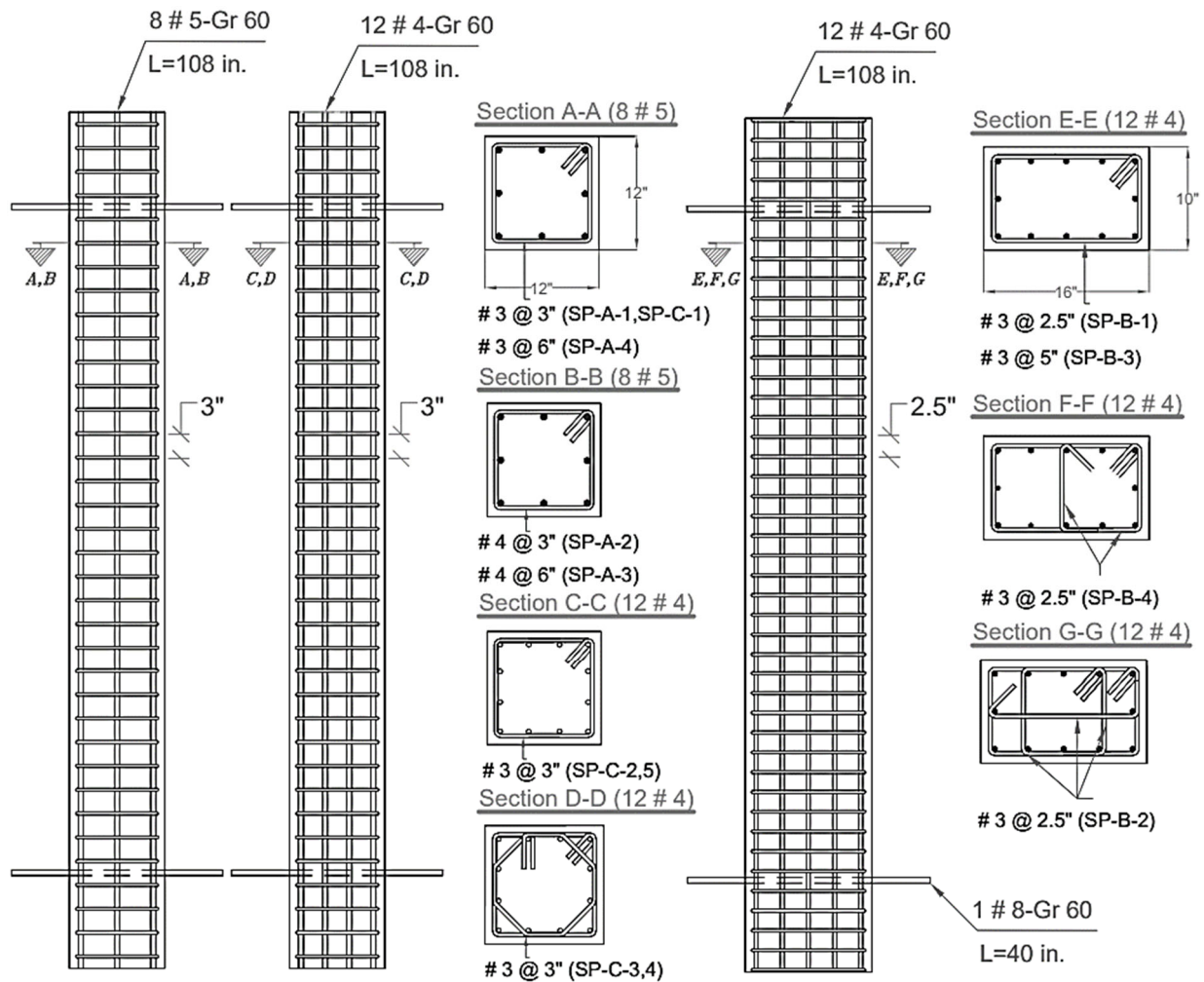


**Figure 2.7** Reinforcement details in elevation views and cross-sections for different columns

## 2.6 Columns Test Setup and Instrumentation

All columns in this study were tested using an enormous universal testing machine (UTM) at the University of California, Berkeley PEER laboratory at Richmond, CA. The hydraulic-press machine has a capacity of 17,793 kN [4000 kips] and can accommodate specimens with a maximum length of up to 10.2 m [33.5 ft] for compression tests and about 6 m [19.7 ft] for tension. A schematic drawing and actual photographs of the UTM and typical columns setup are shown in Figures 2.8 and 2.9, respectively.

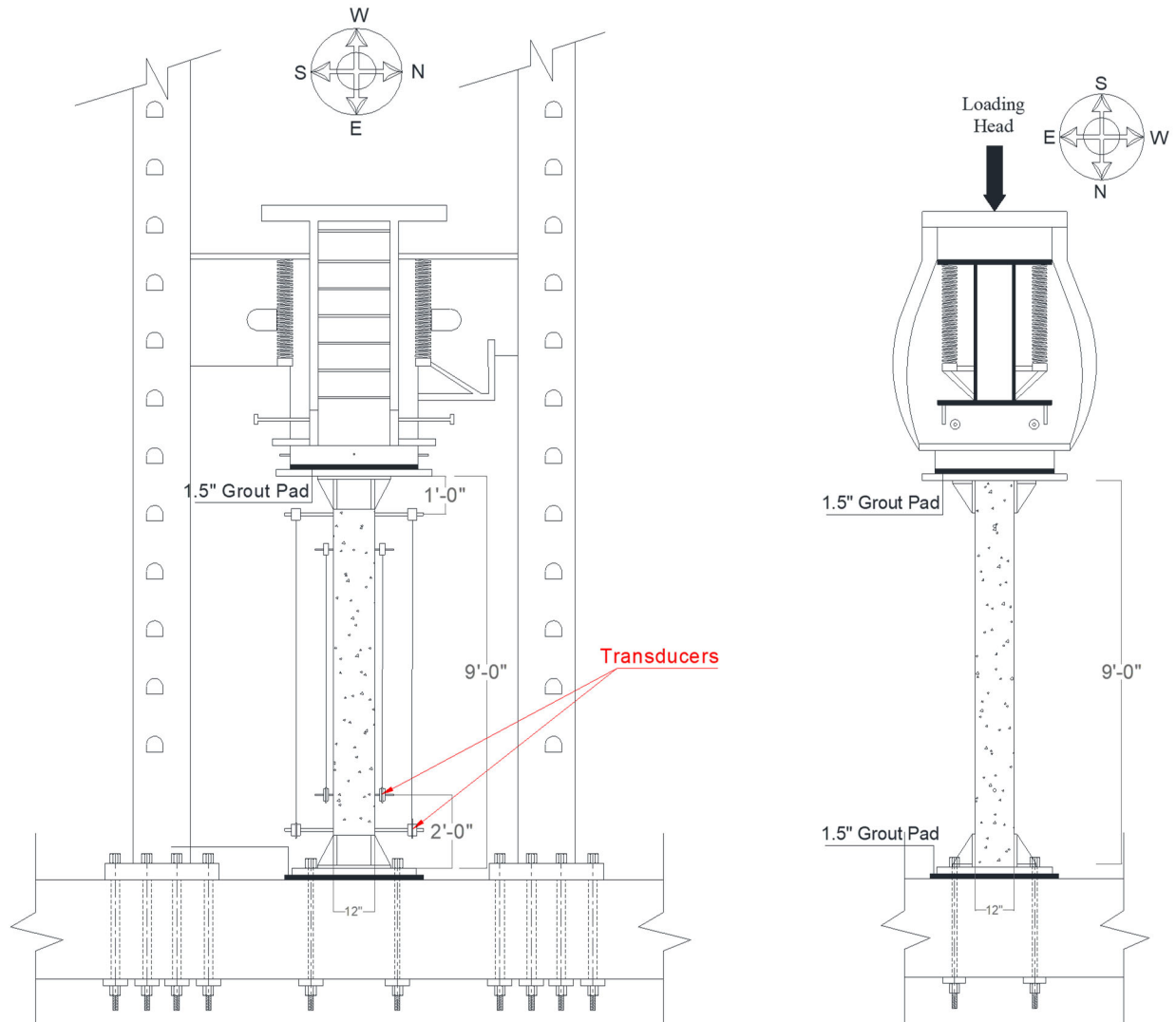


**Figure 2.8** Schematic drawing of the PEER UTM and typical test setup and instrumentation

In Figure 2.7 in the previous section, the typical geometry and the reinforcement detailing for columns with square and rectangular cross sections are shown along with two #8 ( $\phi 25$ ) rebars that were placed laterally in each column. The two big rebars were also accompanied by four small

rods and all were weaved through the rebar cages and formwork at one foot (0.3 m) and two feet (0.6 m), respectively, away from columns' each end (see Figure 2.8) during construction before concrete pouring. The two big rods were used first for columns lifting and handling between horizontal to vertical positions during transportation, setting up, and so on as can be seen in Figure 2.9 for an example of column handling. Then, during testing, both the big and small rods were all used for instrumentation purposes to connect several LVDTs to capture the load-deformation relationship of the columns as illustrated in Figures 2.8 and 2.9. The distance between the two big rods at the ends was around 7 ft (2.13 m). Two LVDTs were mounted to the #8 ( $\phi 25$ ) rods and named big rods (BR) for results discussion in later chapters. The four additional threaded rods (two at the top and two at the bottom) with a diameter of 3/8 in (9.5 mm) were located 2 ft (0.61 m) from the top and bottom of the column for capturing deformation along approximately 5 ft (1.52 m) of the columns' height. The four LVDTs mounted to these threaded rods are referred to as small rods (SR) later in the discussion. All six LVDTs were positioned on the north and south sides for columns with square cross-sections and east and west sides with rectangular cross-sections.

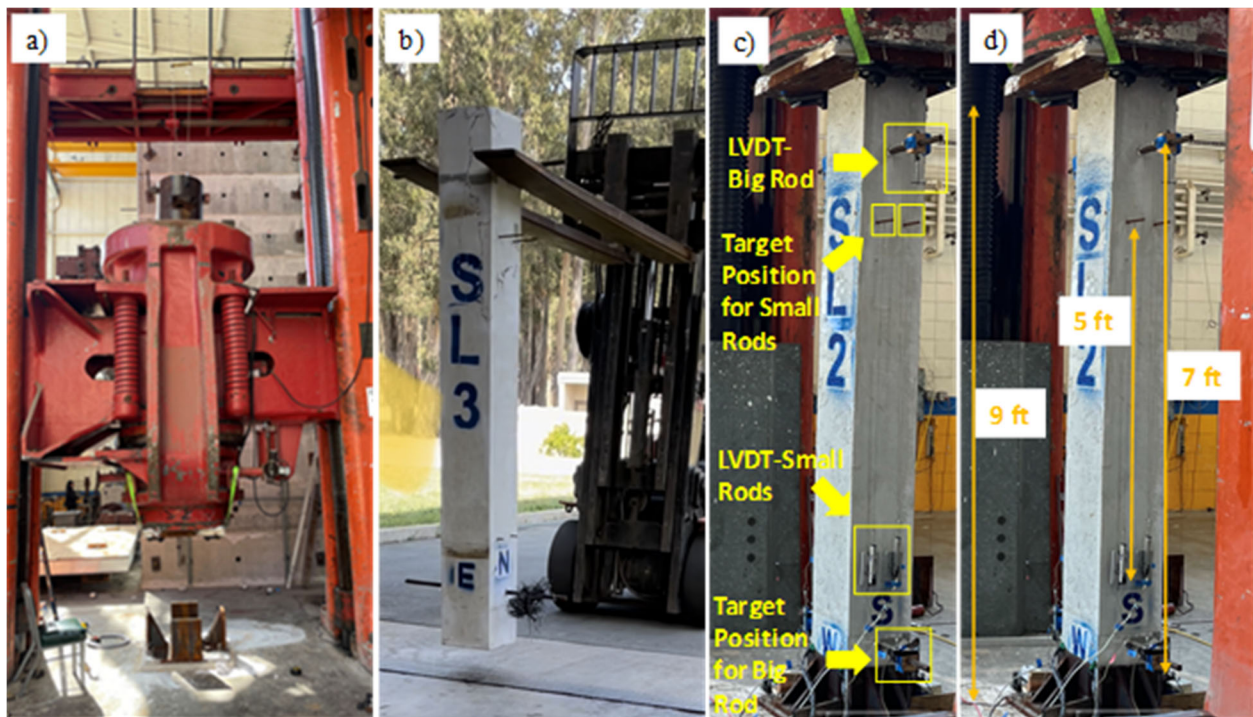


**Figure 2.9** Actual photographs of: (a) the 4,000-kip PEER UTM and load frame; (b) forklift handling of one of the columns using the #8 lifting bars; (c) location of the LVDTs at one of the columns sides; and (d) dimensions of the gage lengths captured by LVDTs and string pots

Steel end plates were grouted at the floor and the bottom of the loading head to have uniform stress distributed on the surface. Vertical brackets were placed at the bottom plate to hold the column in position and to prevent instability while testing, again as illustrated in Figure 2.8. Besides the six LVDTs discussed above, two string potentiometers, that are referred to as SP thereafter, were located on the east and west sides, and attached to the end plates to capture the relative displacement of the machine head, or to some extent, the axial deformation along the full column height. All six LVDTs and the two string pots captured the compressive shortening during testing where strain was calculated later by dividing the shortening of each LVDT by its respective gage length, i.e. ~5 ft for SR, 7 ft for BR, and 9 ft for SP (1.52 m, 2.13 m, and 2.74 m).

In addition to the LVDTs and string pots used for estimating axial strains, about 20 to 36 rebar strain gages were used in each column and were placed at various sections and locations on both transverse and longitudinal reinforcement. The rebar strain gages locations and details are provided later in Chapter 4 as part of the columns behavior discussion. It is also noted that for few selected columns, concrete surface strain gages were used and placed on the columns' surface in longitudinal and transverse directions to capture the concrete's behavior under the applied loading. The strains captured by the concrete gages for the selected instrumented columns are also discussed later in Chapter 4.

### **3 MATERIAL TESTS RESULTS AND MODULUS OF ELASTICITY**

More than a total of 135 cylinders of 3 × 6 in (75 × 150 mm) size were tested under uniaxial compressive loading in order to obtain the UHPC strength and full stress-strain relationships. It was then possible to extract the data for the modulus of elasticity from the obtained full stress-strain curves. In this research study, the modulus of elasticity is calculated as a best-fit linear approximation of stress-strain regions 0-80%, 0-30%, and 10-30% of the compressive strength. This chapter presents the stress-strain relationships and summary of the results of the modulus of elasticity for all three types of UHPC previously presented in Chapter 2. It is noted that due to the large number of tested cylinders, the modulus of elasticity was simply captured through the monotonic stress-strain curve slope without performing the ASTM-suggested loading-unloading cycles. Nevertheless, the authors are currently conducting another side study that focuses on evaluation and assessment of UHPC modulus of elasticity using both ASTM and monotonic testing, but results of that ongoing study is out of the scope of this report and not presented.

#### **3.1 Data Processing and Interpretation**

The testing setup used for all UHPC material (compression) tests was same as previously explained in Chapter 2. Three LVDTs, positioned 120° from each other around the cylinder, were used to capture the axial deformation under compressive loading. The average of the three LVDT recordings was divided by the actual height of the specimen after the saw-cutting and grinding to obtain strain values. As mentioned earlier, this study uses three best-fit linear approximations regions of the stress-strain curve to determine the modulus of elasticity. The region from 0-80% of compressive strength was taken to determine the modulus of elasticity using almost the entire curve, avoiding the nonlinear close to peak or post-peak part of the curve. The region from 0-30% of the strength was taken to incorporate the effect of the loading head adjustment to the specimens, if any. The third region, between 10 and 30% of the ultimate load, was used to obtain the modulus of elasticity in line with what was suggested by Graybeal (2005). Most likely, this region would not have any adverse loading effects like 0-80% and 0-30% of compressive strength captures.

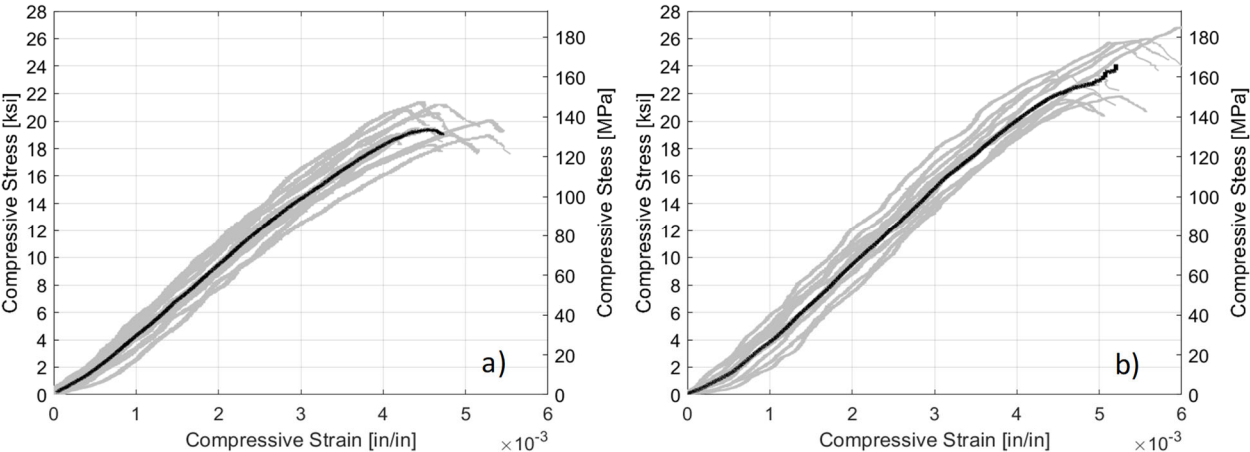
#### **3.2 Results from Type A Cylinders**

Figure 3.1 and Table 3-1 provide the results and summary of compressive behavior of the Type A UHPC cylinders. As shown in Table 3-1, the relatively highest modulus of elasticity value was

obtained using the best-fit approximation of the stress-strain curve between 10 and 30% of the ultimate load at both 28-day and test-day ages. Furthermore, it can be observed that the modulus of elasticity increased by about 9% for the first and third regions and 3% for the second region, respectively, when 28-day and test-day results are compared. Overall, the values of the modulus of elasticity for this type of concrete vary between 4,500 ksi and 5,000 ksi (31,300-34,800 MPa) for the 28 days of age and 5,300 and 5,500 ksi (32,300-38,000 MPa) for the test-day. Therefore, with the increase in the maturity of the tested cylinders, less variation among the regions can be observed. Also, with the maturity of the cylinders, the UHPC strength increased by approximately 16% between the 28-days and test-day ages, i.e. UHPC still continues to gain strength after 28 days. Figure 3.1 provides all stress-strain relationships taken into consideration when obtaining the average modulus of elasticity for the 28-days and test-day ages.

**Table 3-1** Summary of compression strength and modulus of elasticity values using three different stress-strain regions for Type A cylinders at different ages

Test Results		US Units (ksi)		Metric Units (MPa)	
Age		28 days	Test-day	28 days	Test-day
$f_c$		19.8	23.7	136.6	164.9
Modulus of Elasticity	Region #1: 0-80% $f_c$	4,934	5,380	34,018	37,095
	Region #2: 0-30% $f_c$	4,540	4,685	31,300	32,300
	Region #3: 10-30% $f_c$	5,057	5,525	34,869	38,092



**Figure 3.1** Stress-strain curves of Type A UHPC at: (a) 28-days age, and (b) test day

### 3.3 Results from Type B Cylinders

Similar to Type A results above, the strength and modulus of elasticity were obtained at 28-days age and on the test day as shown in Table 3-2. In addition to these two ages, results at about 3.5 month age (105 days) were obtained and presented in Table 3-2. As it can be noted from Table 3-2, cylinders at all three ages exhibited the highest modulus of elasticity in the region between 10-30% of the compressive strength. Compared to the test-day values, 28-day and 105-day modulus of elasticity values increased by 23% and 15% for the first region, 10% and 6% for the second region, and 15% and 10% for the third region. Overall, the values of the modulus of elasticity for this type of UHPC range between 5,300 and 5,700 ksi (36,700 - 39,800 MPa) at 28 days age, 5,600 and 6,000 ksi (39,100 - 41,500 MPa) at 105 days age, and 5,900 and 6,600 ksi (40,800 - 45,700 MPa) at the test day. Unlike Type A, the results for the Type B cylinders do not show less variation of the modulus of elasticity with the maturity of the tested specimens. Also, with the maturity of the cylinders, the strength continue to grow. Only about 2% increase was observed at 105 days versus a 16% increase at test day when compared to 28 days, respectively. Moreover, Figure 3.2 shows all the obtained stress-strain curves at different ages.

**Table 3-2** Summary of compression strength and modulus of elasticity values using three different stress-strain regions for Type B cylinders at different ages

Test Results		US Units (ksi)			Metric Units (MPa)		
Age		28 Days	105 Days	Test Day	28 Days	105 Days	Test Day
$f'_c$		20.8	21.2	24.1	143.1	146.4	165.9
Modulus of Elasticity	0-80% $f'_c$	5,330.9	5,681	6,552.1	36,756	39,171	45,177
	0-30% $f'_c$	5,397.9	5,604	5,931.4	37,218	38,637	40,897
	10-30% $f'_c$	5,783.3	6,023	6,637.8	39,876	41,529	45,767

### 3.4 Results from Type C Cylinders

Compared to the results of the Type A and Type B cylinders, the modulus of elasticity values of Type C cylinders are the lowest, as it can be noted from the overall values presented in Tables 3-1, 3-2, and 3-3 for Types A, B, and C, respectively. This can be attributed to the ingredients, such as sand and cement, sourced locally for the Type C UHPC compared to the carefully selected ingredients of the fully proprietary mixes of Types A and B UHPC. Furthermore, it is noted that the results presented in Table 3-3 are from the companion cylinders of columns SP-C-1, SP-C-2,

and SP-C-3 only, i.e. material results from the 1% steel fibers or 2% recycled fibers cases are not presented nor included here to keep all material results comparisons consistent for only 2% manufactured steel fibers. Similar to the Type A and B cylinders, the highest values of the modulus of elasticity are captured between 10 and 30% of compressive strength. The difference between the results at 28 days and test day is 28% for the first region, 19% for the second region, and 24% for the third region. Overall, the values of the modulus of elasticity for this Type C UHPC vary between 3,700 to 3,900 ksi (25,900 - 27,200 MPa) for 28 days age, and 4,400 to 4,800 (30,800 - 33,700 MPa) for test day.

Also, with the maturity of the cylinders, the strength significantly increased by 42% at test day relative to the 28-day strength. It is worth noting that strength captured at 28 days of age is not the typical representative strength value for this category of UHPC. As mentioned earlier, cylinders did not go through any treated regimes. All cylinders were placed outside next to the columns to mimic the strength development of the structural elements. Therefore, Type C cylinders went through extreme cold temperatures and large temperature changes since the casting of the columns was in the wintertime in the Reno, NV area. As reported by the vendor, the Cor-Tuf product is particularly sensitive to the curing regime. This can also be concluded when 28-day and test-day strengths are compared. Most likely, the full hydration process was slower due to the freezing of the water particles and it took several weeks for the strength to reach its expected typical values. Moreover, and for completeness, Figure 3.3 shows all the compressive stress-strain curves obtained from Type C cylinders and used for obtaining the average modulus of elasticity at 28 days and test day from the three different regions.

**Table 3-3** Summary of compression strength and modulus of elasticity values using three different stress-strain regions for Type C cylinders at different ages

Test Results		US Units (ksi)		Metric Units (MPa)	
Age		28 days	Test-day	28 days	Test-day
$f'_c$		15.3	21.8	105.5	150.3
Modulus of Elasticity	Region #1: 0-80% $f'_c$	3,832	4,892	26,421	33,734
	Region #2: 0-30% $f'_c$	3,756	4,472	25,900	30,836
	Region #3: 10-30% $f'_c$	3,956	4,892	27,277	33,727

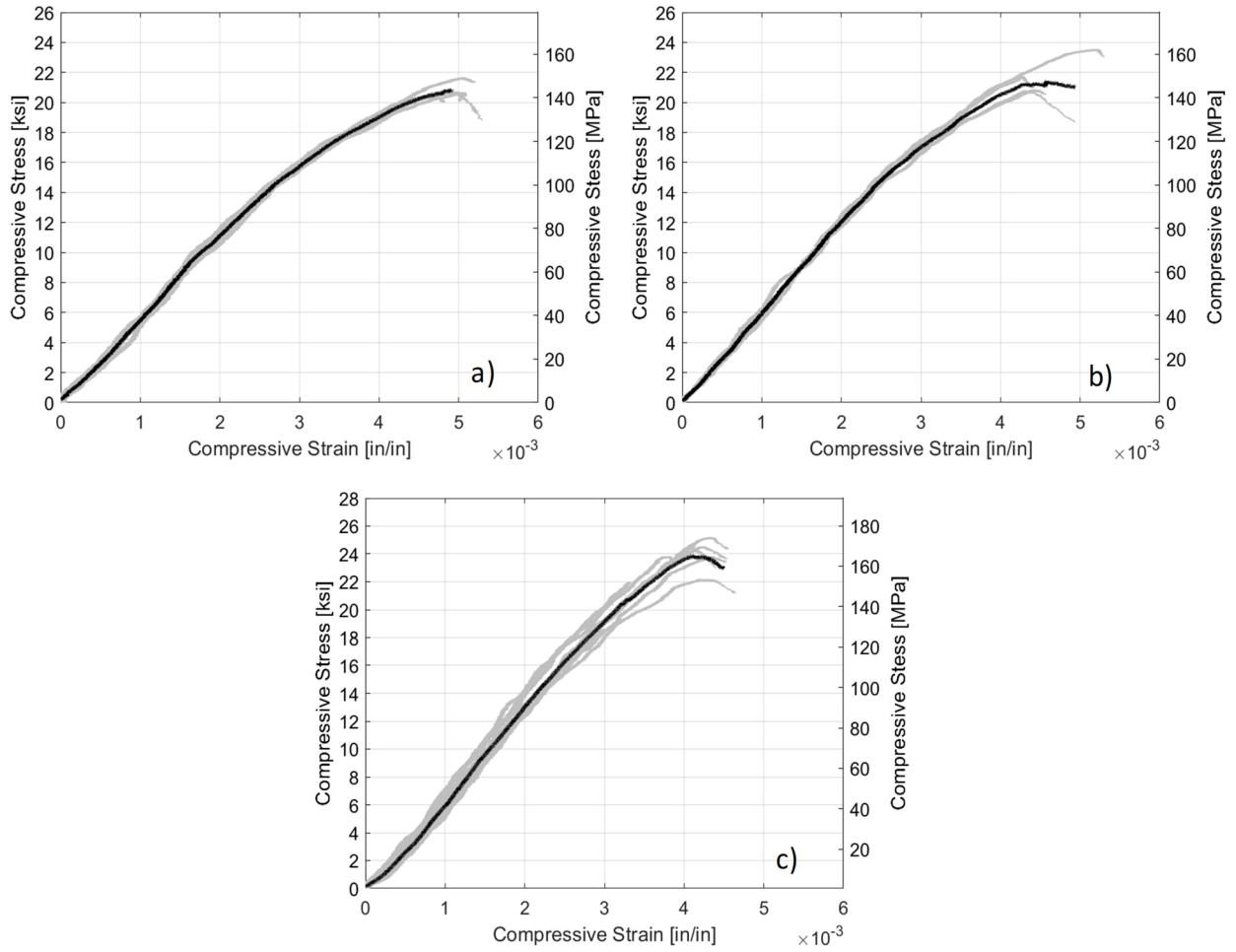


**Figure 3.2** Compressive stress-strain curves of Type B UHPC captured at: (a) 28 days, (b) 105 days, and (c) test day

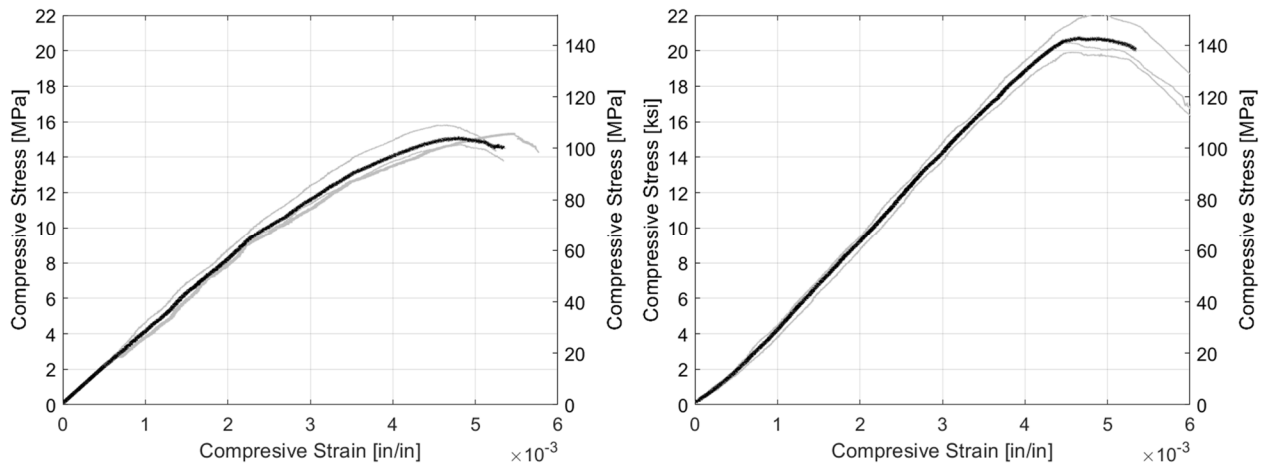


**Figure 3.3** Compressive stress-strain curves of Type C UHPC captured at 28 days (left) and test day (right)

## 4 AXIAL BEHAVIOR OF COLUMNS

This chapter provides all the structural testing results of four Type A, four Type B, and five Type C full-scale UHPC columns. Both global response, i.e. force versus axial deformation and strain, and local response, i.e. the strain propagation of the longitudinal and transverse reinforcement during the testing, are presented and discussed. The yielding of the reinforcing bars, eccentricity due to construction or test setup errors, and local buckling effects are also discussed in this chapter, when relevant.

It is noted as mentioned previously, six LVDTs and two string potentiometers were used to capture the columns' axial shortening under pure axial loading. The average from the two LVDTs connected to the big rods (BR), four LVDTs connected to the small rods (SR), and the two string potentiometers (SP) between the machine head and base plates, were all obtained in order to estimate the axial deformation and in turn, the compressive axial strain of the tested columns.

Overall, the columns with different UHPC types of emerging mixtures varied also the transverse reinforcement to confirm whether the current ACI detailing requirements are necessary for UHPC columns or can be further relaxed. As such, each group of columns from a different UHPC comprised both ACI compliant and non-compliant columns. This is inspired by the many ongoing calls that UHPC structural design should leverage the improved performance associated with the steel fibers, which is known to have an immediate impact on shear strength but no previous work has yet comprehensively tested this hypothesis for confinement effects. In this study, exploring ways of relaxing transverse reinforcement requirements included two main practices: (1) a large transverse reinforcement spacing that deliberately violates the recommended value of 6 or less for the spacing to longitudinal bar diameter ( $s/d_b \leq 6$ ); and (2) avoiding the need to constrain rebars using stirrups or cross-ties corners when lateral distance to closed properly constrained bars exceed 6 inches. In this chapter, the analyzed axial behavior of those non-compliant columns is meant to shed some light on whether current ACI 318 transverse reinforcement provisions can be relaxed for UHPC columns.

### 4.1 Type A Columns

All four columns made out of Type A UHPC had square cross-sections, as noted earlier in Chapter 2 and test matrix discussions. All SP-A columns had 2% of the steel fibers ratio, but their transverse

reinforcement ratios differed in terms of the spacing and the size of the transverse rebars. Specimens SP-A-1 and SP-A-2 were ACI compliant columns, while SP-A-3 and SP-A-4 are considered non-ACI compliant columns due to the larger spacing of transverse reinforcement when compared to the ACI 318-19 requirements.

#### 4.1.1 Summary of Key Results

It is mentioned earlier that per the properly reinforced detailing, SP-A-1 and SP-A-2 were considered ACI compliant columns due to the 3 in (76.2 mm) transverse reinforcement spacing, i.e.  $s/d_b = 3/0.625 = 4.8$ , which conforms with the  $s/d_b \leq 6$  requirement. Meanwhile, SP-A-3 and SP-A-4 are not considered ACI compliant where the 6 in (152.4 mm) spacing of the transverse reinforcement led to a non-compliant  $s/d_b$  value of 9.6 ( $>6$ ). Furthermore, SP-A-1 and SP-A-4 had #3 ( $\phi 10$ ) transverse rebars while SP-2 and SP-3 had #4 ( $\phi 13$ ) transverse rebars. All Type A columns were instrumented with six LVDTs on the north and south sides and two string pots on the west and east sides. The four columns were tested through failure using the setup and methods previously discussed in Chapter 2, and a summary of the key results from Type A columns tests is provided first in Table 4-1 in this subsection before detailed results are discussed next. The table summarizes the maximum axial load capacity, strain at peak force, and estimated stiffness for all four columns. Details on how the strain at peak and stiffness values were obtained are provided through the force versus deformation and strain discussions in following subsections. It is noted that due to the adopted construction methods, the depth of columns was not necessarily achieved at exactly 12 in, and as such, the actual cross-section area of each column is reported in the results table as well.

**Table 4-1** Summary of key test results of Type A UHPC columns

<b>Column ID</b>	<b>Cross-Section Area, in<sup>2</sup> (cm<sup>2</sup>)</b>	<b>Maximum Axial Force, kips (kN)</b>	<b>Strain at Peak</b>	<b>Stiffness, kip/in (kN/mm)</b>
SP-A-1	155.9 (1,005.6)	2,504 (11,139)	0.0037	7,601 (1,331)
SP-A-2	144.8 (934.2)	2,389 (10,625)	0.0033	8,595 (1,505)
SP-A-3	140.6 (906.8)	2,105 (9,365)	0.0030	8,924 (1,563)
SP-A-4	143.9 (928.2)	1,904 (8,469)	0.0029	8,730 (1,529)

#### 4.1.2 Damage Progression

The Type A columns' modes of failure are presented in Figure 4.1. All the columns were subjected to axial concentric loading up to the complete loss of the columns' axial capacity. During the loading process, it was observed that columns had some minor crushing of concrete at the top and the bottom. These crushing signs were due to imperfections during the construction, where the columns ends formwork were not perfectly parallel and some longitudinal rebars were slightly shifted in one side more than other sides. Three out of the four columns did not have the perfectly parallel top and bottom surfaces and experienced some minor eccentricity effects as observed in the load versus longitudinal rebars strain graphs later. Only SP-A-3 did not have any obvious eccentricity.

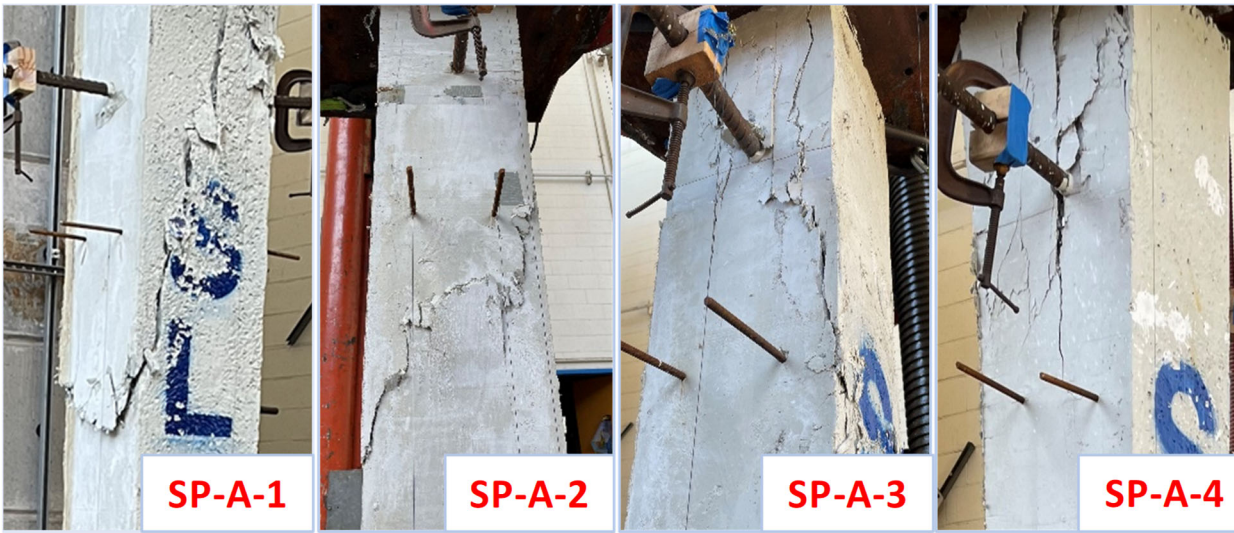


**Figure 4.1** Mode of failure of the four different Type A columns after testing

The first major damage was the spalling of the cover concrete, visually noticeable by the vertical splitting of the concrete and the slight reduction in load resistance. Due to the high compressive force in SP-A-3 and SP-A-4 causing bulging and tensile stresses in transverse reinforcement, some of the observed lateral rebars yielded, becoming soft and less effective in providing confining stress to the core concrete. At the end of the testing, some transverse bars were fractured under the high tensile stresses at the failure load due to the local buckling of one or multiple longitudinal rebars. Most of the columns had a major crack opening starting from the top. Overall, the longitudinal rebars yielded before the concrete crushing in all the columns. Longitudinal rebars buckling was observed in SP-A-3 and SP-A-4. However, in SP-A-1 and SP-A-2 no longitudinal

rebar buckling was inferred and none of the instrumented transverse rebars yielded, implying that transverse reinforcement in these two specimens was not fully engaged, as discussed later in force versus strain relationships.

#### *4.1.3 Force versus Deformation Relationships*

Figure 4.2 shows the average axial force versus deformation relationships obtained for the different Type A columns from three sets of measurements, i.e. average from two BR LVDTs, average from four SR LVDTs, and average from two string pots (SP). The figure also provides an overall average force-deformation curve from all sets combined. According to Figure 4.2, it is noted that SP-A-1 has the highest deformation captured and therefore softer load-deformation curve leading to the lowest stiffness when compared to other specimens. This might be attributed to the improper setup of the instrumentation of the first specimen. As a consequence, the deformations captured might have been slightly inaccurate. All other specimens had similar deformations and, therefore, stiffness values, which should be expected based on the similar material and geometry within all four columns. Such observation can be properly noted from the values reported in Table 4-1 that show a stiffness value of about 7,600 kip/in for SP-A-1 versus values in the range of 8,600-8,900 kip/in for other specimens.

#### *4.1.4 Force versus Axial Strain Relationships*

In order to compare all four columns' behavior during the axial loading, the force versus strain graphs were also obtained and presented in Figure 4.3. The strains calculated from the different measurement sets used different gage length based on instrumentations setup, and as such, the strains from SR and BR are very close as they both were not affected by the deformations at column head or other setup pieces. Even though SP-A-2 had a higher percentage of the transverse reinforcement when compared to SP-A-1, due to using #4 ( $\phi 13$ ) size of rebar instead of #3 ( $\phi 10$ ), yet SP-A-3 exhibited a relatively lower failure load than SP-A-1 and higher strain capacity. One possible reason for this unexpected reduction in the capacity can be attributed to the eccentricity effects, which are better discussed in the context of both longitudinal and transverse reinforcement strains in the next subsection. Such eccentricity effect might have prevented SP-A-2 from performing better in terms of strain capacity, which would be expected due to the higher confining effect that should be provided by #4 ( $\phi 13$ ) rebars when compared to #3 ( $\phi 10$ ).

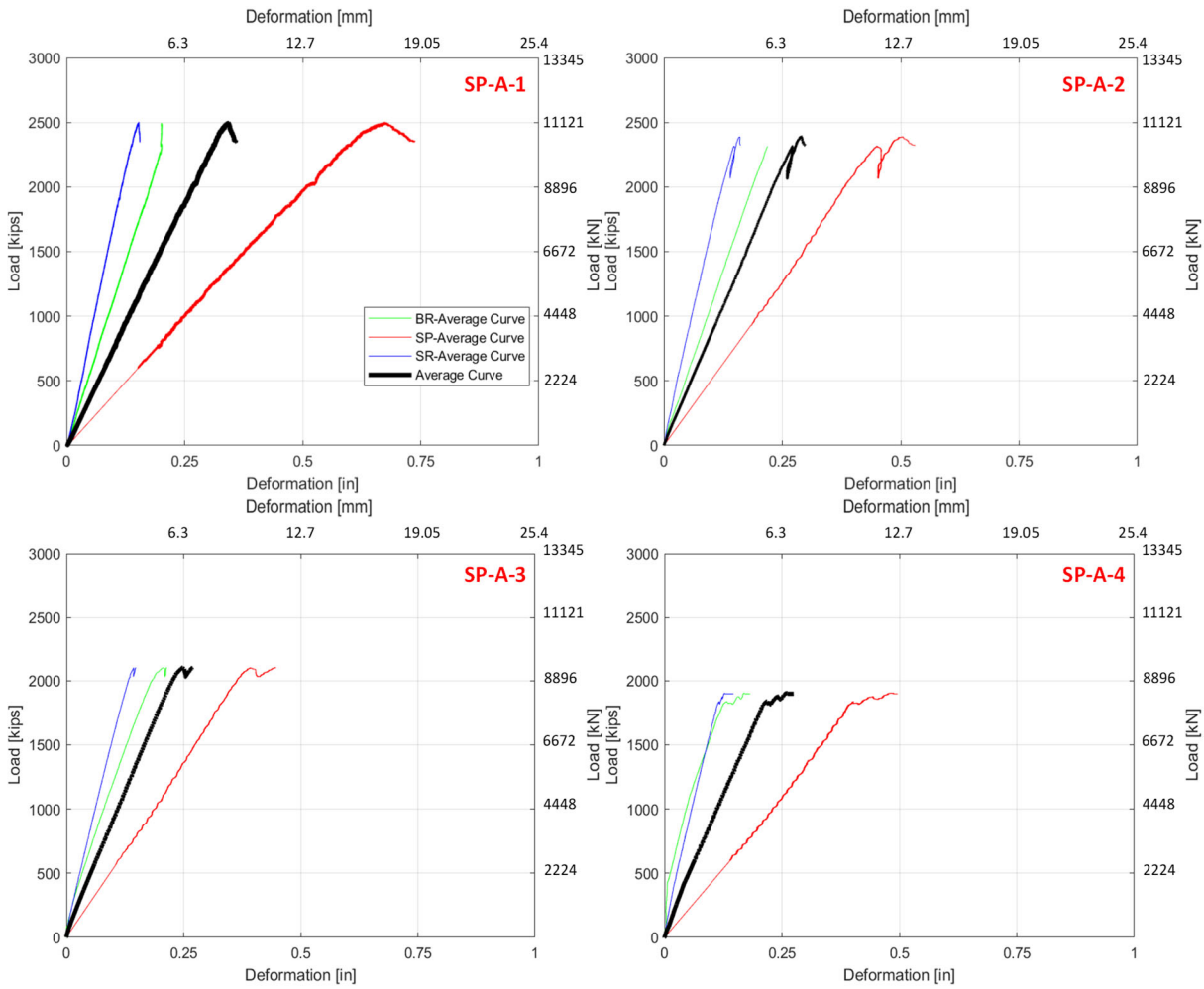


**Figure 4.2** Force versus deformation relationships for Type A columns using the three different LVDTs or SP sets

Furthermore, both SP-A-1 and SP-A-4 had the same diameter of the transverse reinforcement bars, but the spacing of SP-A-4 was double the spacing of SP-A-1. The spacing significantly affected the columns' behavior, where the axial load capacity of SP-A-1 was 24% higher when compared with SP-A-4. Similarly, the axial capacity of SP-A-2 was 13% higher than the capacity of the SP-A-3, where both had size #4 ( $\phi 13$ ) of the transverse bars, but SP-A-3 had double the spacing when compared with SP-A-2.

Also, column SP-A-3 outperformed column SP-A-4 regarding the maximum failure load (about 11% increase). As mentioned earlier, SP-A-3 has transverse reinforcement bars #4 ( $\phi 13$ ), while SP-A-4 has #3 ( $\phi 10$ ). A bigger diameter of the rebar will increase the confinement effects on the core and improve the specimens' structural performance overall in the case of columns with the 6 in spacing. Thus, in the case of non-ACI compliant columns where the spacing of transverse

reinforcement is higher than allowed, the diameter of the rebar might make a difference in terms of the axial load capacity. However, the transverse rebars' spacing overall significantly affects the columns' axial capacity, and as such, conforming with the  $s/d_b \leq 6$  ACI requirement would be recommended for UHPC columns.

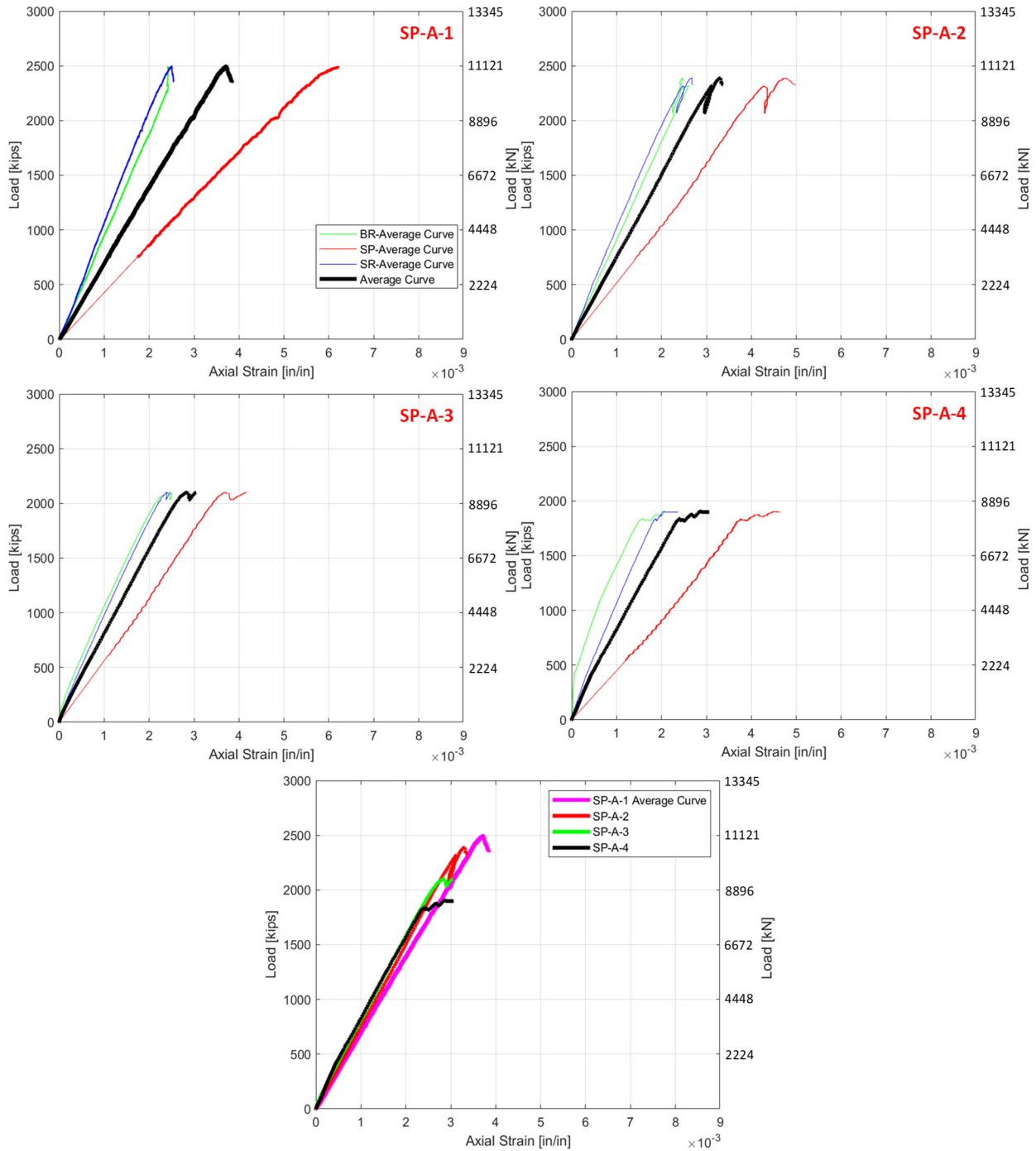


**Figure 4.3** Force versus axial strain for all four Type A UHPC columns as obtained from different measurement sets along with comparison of the overall average curves of all columns

#### 4.1.5 Longitudinal and Transverse Reinforcement Strains

The strain values recorded on the longitudinal and transverse rebars suggest that all columns, except column SP-A-3, experienced eccentricity where strains were not uniform at opposite sides of those columns. Figure 4.4 shows the force versus the strain measured at two opposite corner longitudinal rebars and at three different levels along the columns height for all Type A columns. Similarly, Figure 4.5 shows the force versus strain measured at selected transverse reinforcement levels along the column height for Type A columns. All strain values in Figures 4.4 and 4.5 are expressed in microstrain values (i.e. strain  $\times 10^6$ ). The deviation of the strain among longitudinal and transverse reinforcement in Figures 4.4 and 4.5 confirms that for some columns, one side sustained more loading than opposite side due to eccentricity the could be a result of the construction and setup imperfections.

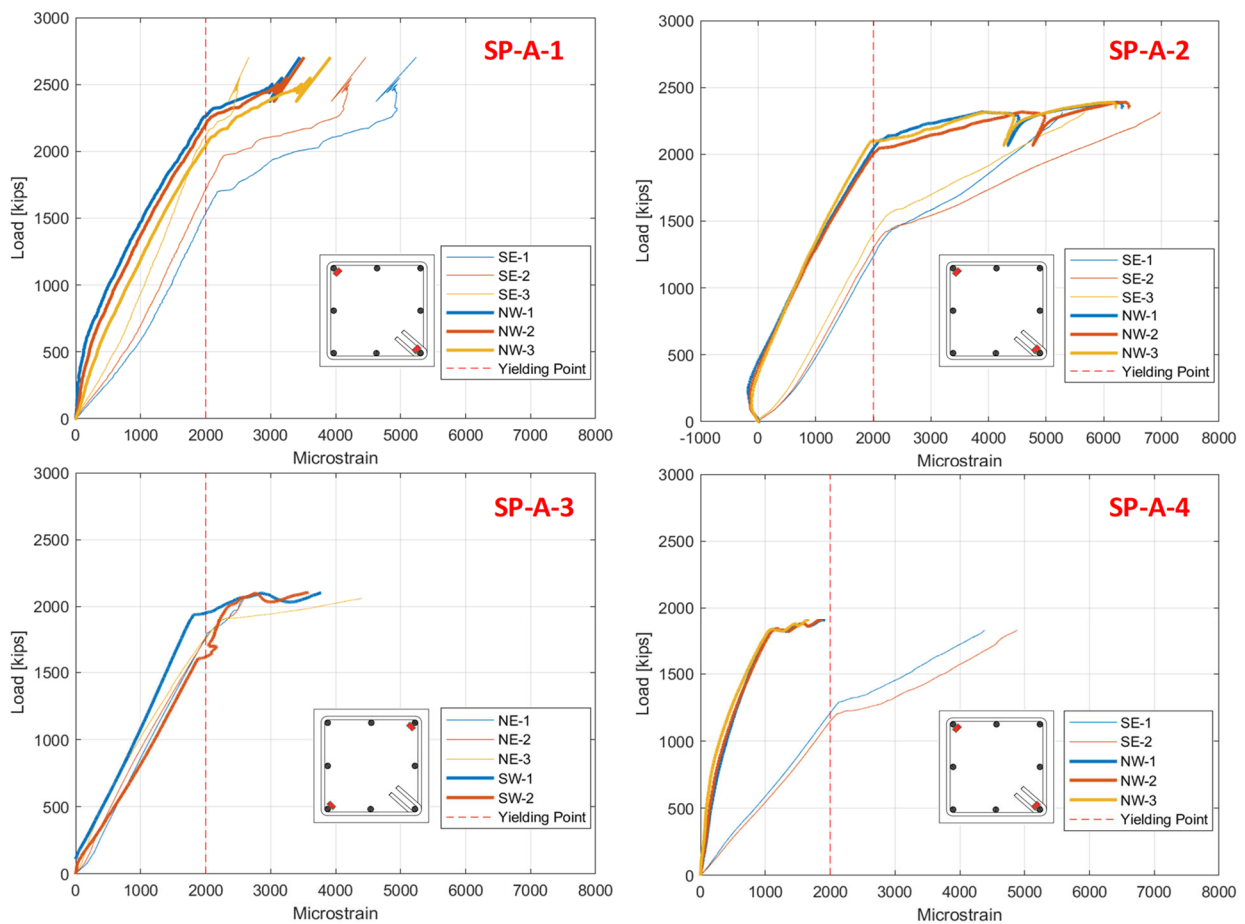


**Figure 4.4** Force versus longitudinal rebars strain at different locations and heights along height in all four Type A columns

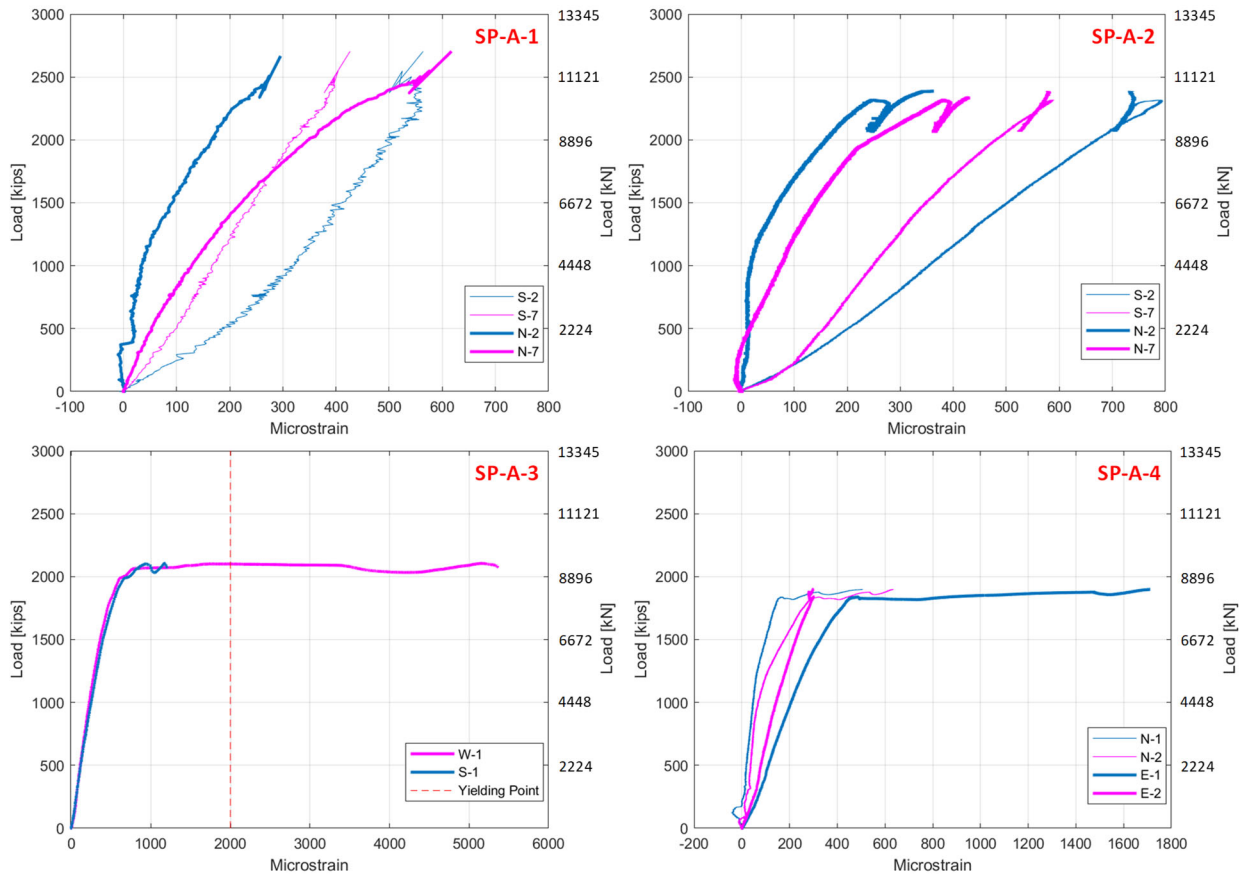


**Figure 4.5** Force versus selected transverse rebar strain at different locations and heights along height in all four Type A columns

Also, in some columns, the strain gages installed on the lateral transverse reinforcement, as shown in Figure 4.5, indicated that one or two transverse reinforcement bars yielded due to the high tensile stresses in the steel provided by the dilatation of the core concrete. In the case none of the instrumented lateral bars reached the yield point implies either that very localized failure happened outside the instrumented stirrups or that the transverse reinforcement was not fully engaged due to failure dictated by early local buckling of the longitudinal rebars in between certain stirrups, which happened in SP-A-1 and SP-A-2.

In addition to the strain results shown in the figures above, the load value at the onset of yielding in the different longitudinal rebar is noted and summarized in Table 4-2. The onset of yield loading is also presented as a percentage of the maximum achieved load (i.e. load at failure) for the different columns. The load values and percentages also confirm that not all longitudinal bars yielded at the same time due to eccentricity.

**Table 4-2** Load values at onset of yielding strain of the longitudinal bars in Type A columns

Column ID			SP-A-1	SP-A-2	SP-A-3	SP-A-4	
Failure Load [kips]			2,504	2,389	2,105	1,904	
Load at onset of yield	Corner Rebars	NW	kips	2,051	2,008		-
			% of failure	82	84		-
		SE	kips	1,545	1,235		1,151
			% of failure	62	52		60
		NE	kips			1,752	
			% of failure			83	
	SW	kips			1,617		
		% of failure			77		
	Middle Rebars	N	kips			1,682	1,859
			% of failure			80	98
		W	kips				
			% of failure				
		E	kips			1,678	
			% of failure			80	
Eccentricity Effect?			YES	YES	NO	YES	

## 4.2 Type B Columns

Type B columns are the ones made out of the CNF-enhanced UHPC, which all four columns had rectangular cross-sections, as noted earlier in Chapter 2 and the test matrix details. All SP-B columns had 2% of the steel fibers ratio, but their transverse reinforcement differed in terms of the spacing, configuration, and ACI detailing compliance. Specimens SP-B-2 and SP-B-4 were ACI compliant columns, while SP-B-1 and SP-B-3 were considered non-ACI compliant columns due to the lack of any cross-ties or internal stirrups (i.e. only four out of 12 rebars were constrained at the corner of stirrups) and additionally, the large spacing of transverse reinforcement in SP-B-1 (5 in spacing corresponds to  $s/d_b$  value of 10, which well exceeds the ACI limit of  $s/d_b = 6$ ).

### 4.2.1 Summary of Key Test Results

Per the properly reinforced detailing explained earlier, SP-1 and SP-3 had less transverse reinforcement, while SP-2 had more when assessed against ACI detailing. Only SP-4 followed the

just required reinforcement detailing. SP-1 had a 5 in (127 mm) spacing without any additional hoops or ties. SP-3 had the same transverse rebar configuration as SP-1 but with 2.5 in (63.5 mm) longitudinal hoop spacing. The overly reinforced column, SP-2, had rectangular hoops and crossties tying the middle bars on the opposite sides of the shorter dimension using 2.5 in (63.5 mm) spacing as shown earlier in the columns cross-section drawings in Chapter 2. Similarly, the transverse reinforcement configuration of SP-4 had crosstie on the longitudinal rebar due to more than 6 in (152 mm) space between the corner and middle bars (ACI 318 requirement).

All Type B columns were instrumented with six LVDTs on the west and east sides; therefore, the position of the LVDTs for the Type B columns differed from the positions suitable for the Type A columns, while the string pots were the same as for the Type A columns (one string pot on west and east sides). All columns were tested through failure using the testing methods presented in Chapter 2 and Table 4-3 herein summarizes the maximum axial load capacity, strain at peak force, and estimated stiffness for all four Type B columns.

**Table 4-3** Summary of key test results of all four Type B columns

<b>Column ID</b>	<b>Cross-Section Area, in<sup>2</sup> (cm<sup>2</sup>)</b>	<b>Max. Axial Force, kips (kN)</b>	<b>Strain at Peak</b>	<b>Stiffness, kip/in (kN/mm)</b>
SP-B-1	170.7 (1,101)	1,796 (7,990)	0.0027	10,330 (1,809)
SP-B-2	163.3 (1,054)	2,503 (11,134)	0.0031	11,306 (1,980)
SP-B-3	168.7 (1,088)	2,186 (9,723)	0.0027	10,243 (1,794)
SP-B-4	167.9 (1,083)	2,770 (12,320)	0.0031	11,059 (1,937)

#### 4.2.2 Construction Challenges

Five batches were needed to construct each of the four Type B columns. Due to the high dosage of the accelerator and the cold weather, specimens had four planes of weakness due to the low flowability and quick setting time of the previously mixed and cast layer. As mentioned earlier, mixing each of the five batches unexpectedly lasted 20-30 minutes more than anticipated. The previous cast layer was hardening when the fresh batch of concrete was poured, preventing proper intermixing between the layers. As a result of poor connections between the layers, the delamination of five layers was observed after the end of the testing, as shown in Figure 4.6, and

later in next subsection in Figure 4.7. Furthermore, due to the low flowability of the cast concrete, honeycombing could be observed on the surfaces of SP-B-2 and SP-B-3 after taking the formwork off. Due to the high transverse reinforcement percentage and low flowability, steel fibers could not pass through the dense reinforcement configuration. Consequently, the steel fibers could not be uniformly dispersed over the height of the column. According to Sbia et al. (2014), the relatively large spacing of the fibers helps the growth of the microcracks. Therefore, using more transverse reinforcement ratio than what would be needed in light of the ACI 318-19 provisions may adversely affect the overall structural performance of the column instead of providing more confinement.

Furthermore, according to Du et al. (2001) and a research study Heshe and Nielsen (1992) mentioned in a research paper by Hosinie et al. (1995), the direction of the pouring UHPC may have a significant effect. As mentioned earlier, the columns tested in this study were horizontally placed, so the pouring of concrete was perpendicular to the loading direction. According to Du et al. (2001) and Heshe and Nielsen (1992), considering the steel fibers' orientation, the pouring direction should be parallel to the loading direction. In this study, however, steel fibers, due to the pouring, were mostly parallel to the loading direction, which may lower the bridging effect at the time of the crack openings. The steel fibers' orientation may not significantly distress Type A and Type C columns. Still, in specimens already exposed to some construction difficulties, the incorrect steel fiber orientation may add additional adverse effects on the overall mechanical behavior of the specimen.

Lack of the steel fibers' bridging effects due to the high percentage of the reinforcement or pouring direction, proper connections between the layers, and inconsistent cross-section over the height of the columns due to the honeycombing led columns SP-B-2 and SP-B-3 to relatively lower capacity or a premature failure as rendered in Table 4-3.

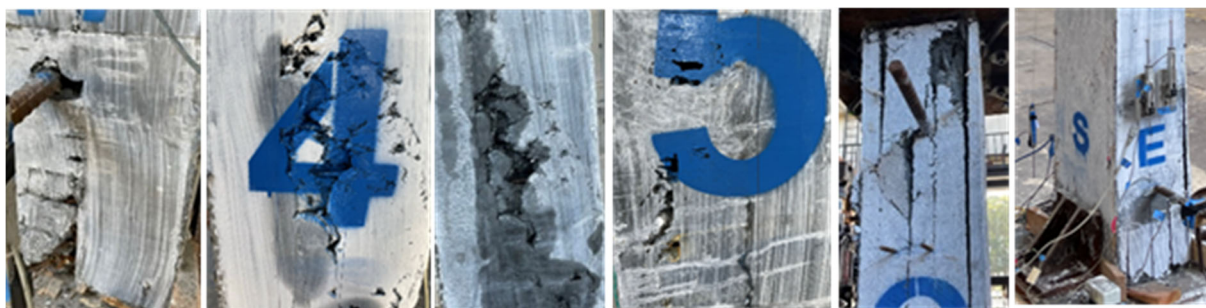


**Figure 4.6** Honeycombs and delamination of Type B columns

### 4.2.3 Damage Progression

Type B specimens' modes of failure are presented in Figure 4.7. All specimens were subjected to axial concentric loading up to the complete loss of the columns' axial capacity. During the loading process, it was observed that columns had some minor crushing of concrete at the top and the bottom. These crushing signs were due to imperfections during the construction, such as varying end positions of the longitudinal rebars. These imperfections led to unparallel ends and slight eccentricity effects, which could be observed in the load versus strain graphs that are shown and discussed later.



**Figure 4.7** Photographs of the Type B UHPC columns failure after axial testing

The first major damage was the spalling of the cover concrete, visually noticeable by the vertical splitting of the concrete and the reduction in load resistance. Due to the higher compressive force, only in SP-B-3, one of the transverse bars yielded and was incapable of providing effective confining stress to the core concrete.

The honeycombing observed in SP-B-2 and SP-B-3 reduced the cross-section in some of the columns' height areas. These reduced sections and holes led to some local stress concentration leading these two specimens to premature failures. Moreover, as shown in Figure 4.7, SP-B-3 and SP-B-4 had delamination issues. The improper bond between all five layers was the main damage pattern in both specimens. Even though the delamination affected the failure modes, both columns achieved high axial capacity compared to the rest of the specimens.

#### 4.2.4 Force versus Deformation Relationships

As done before for Type A columns, different measurement sets were used to obtain axial deformation for Type B columns. Figure 4.8 provides the average force versus deformation relationships from each measurement set along with the overall average curve from all sets combined. According to the force versus deformation relationships shown in Figure 4.8, the highest stiffnesses were achieved by SP-B-2 and SP-B-4. Honeycombing and the delamination might have an adverse impact on the stiffnesses of the SP-B-1 and SP-B-3, where they had more deformation during the lower force applied.

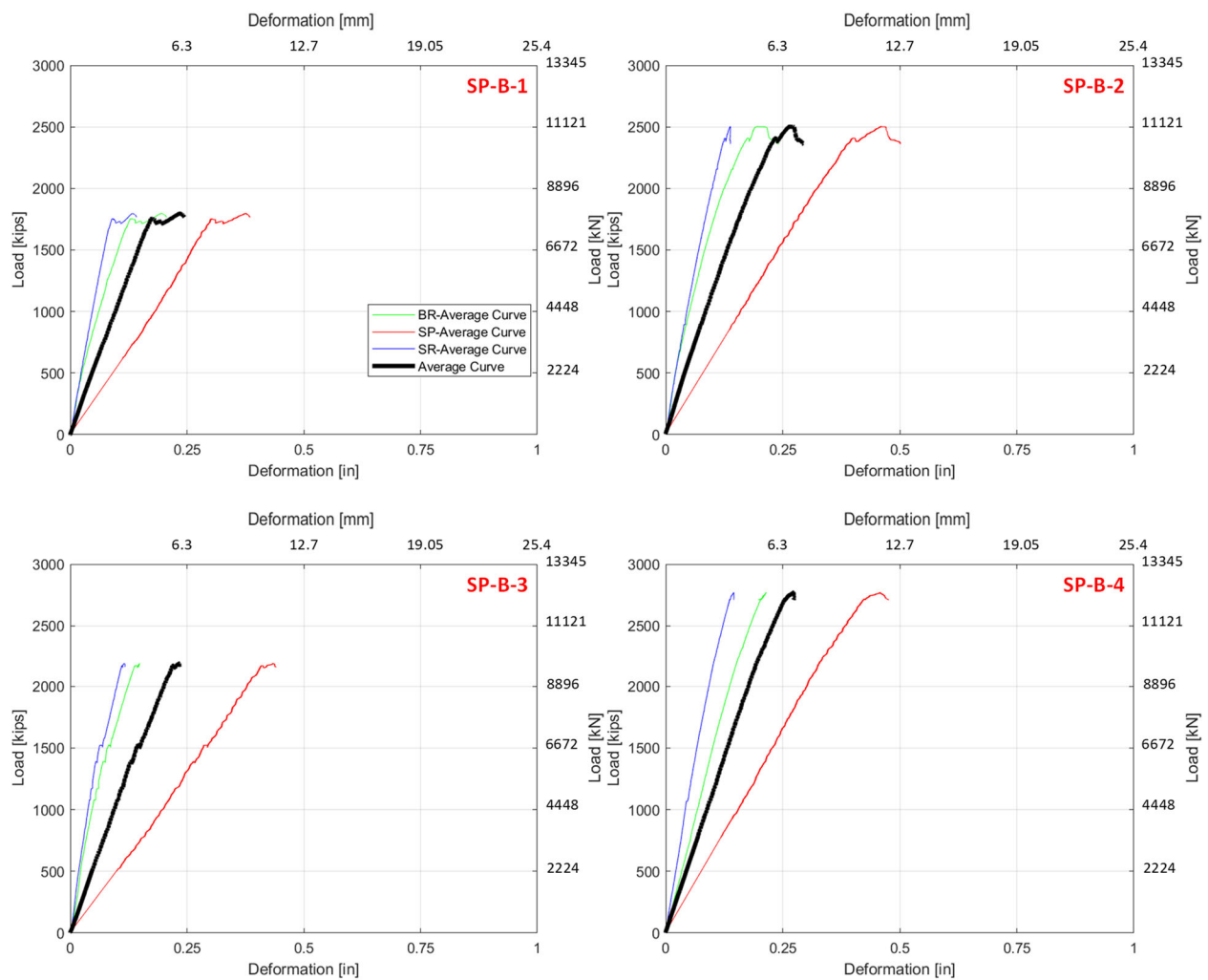


**Figure 4.8** Average force versus deformation relationships for all Type B columns using different LVDTs and SP measurement sets

#### 4.2.5 Force versus Axial Strain Relationships

Figure 4.9 compares the average obtained axial strain for all four Type B columns. As shown in the figure, SP-B-1 and SP-B-3 had the lowest strain capacity, which was expected due to the lowest confinement ratios.

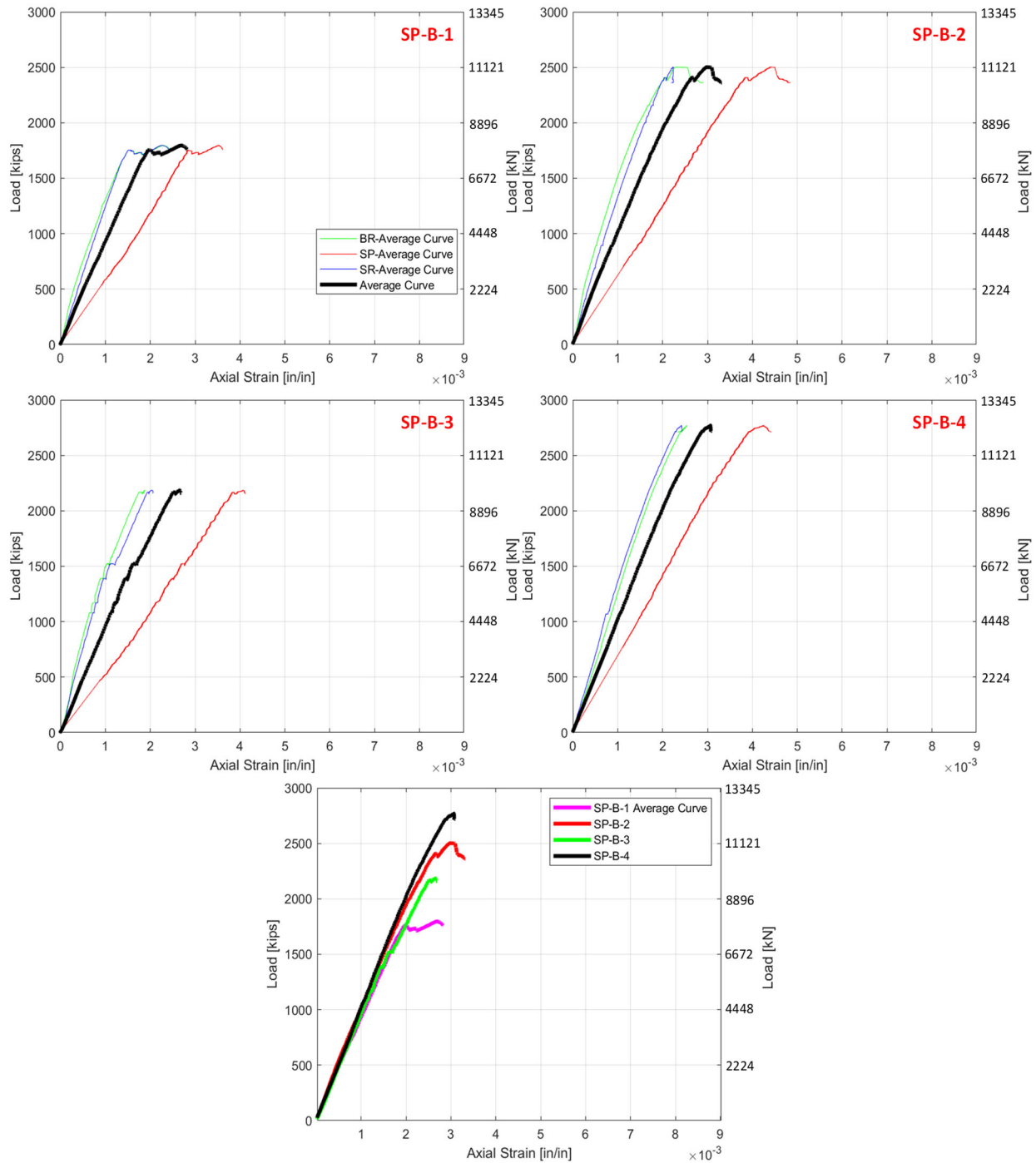


**Figure 4.9** Force versus axial strain for all four CNF-enhanced Type B UHPC columns

Due to the better flowability and fewer observed honeycombing on the surface, SP-B-3 and SP-B-4 performed well in terms of the achieved failure load. Also, SP-B-2 exhibited high axial strain capacity, which was expected due to over-confinement. It is worth noting that the SP-B-4 had 35%, 10%, and 21% higher axial load capacity when compared to SP-B-1, SP-B-2, and SP-B-3, respectively. As mentioned earlier, SP-B-1 and SP-B-2 had a major construction defect which led to premature failure. In the case of SP-B-3, SP-B-4 had the addition of the tie, which helped with confining the core concrete and therefore increased deformation and strain capacity. Like in the case of Type A columns, the transverse reinforcement's higher spacing significantly affects the axial load capacity, which applies to SP-B-1 when compared to SP-B-3.

#### 4.2.6 Longitudinal and Transverse Reinforcement Strains

The force versus strain values recorded on the various corner and middle longitudinal rebars and transverse stirrups are shown in Figures 4.10, 4.11, and 4.12, respectively.

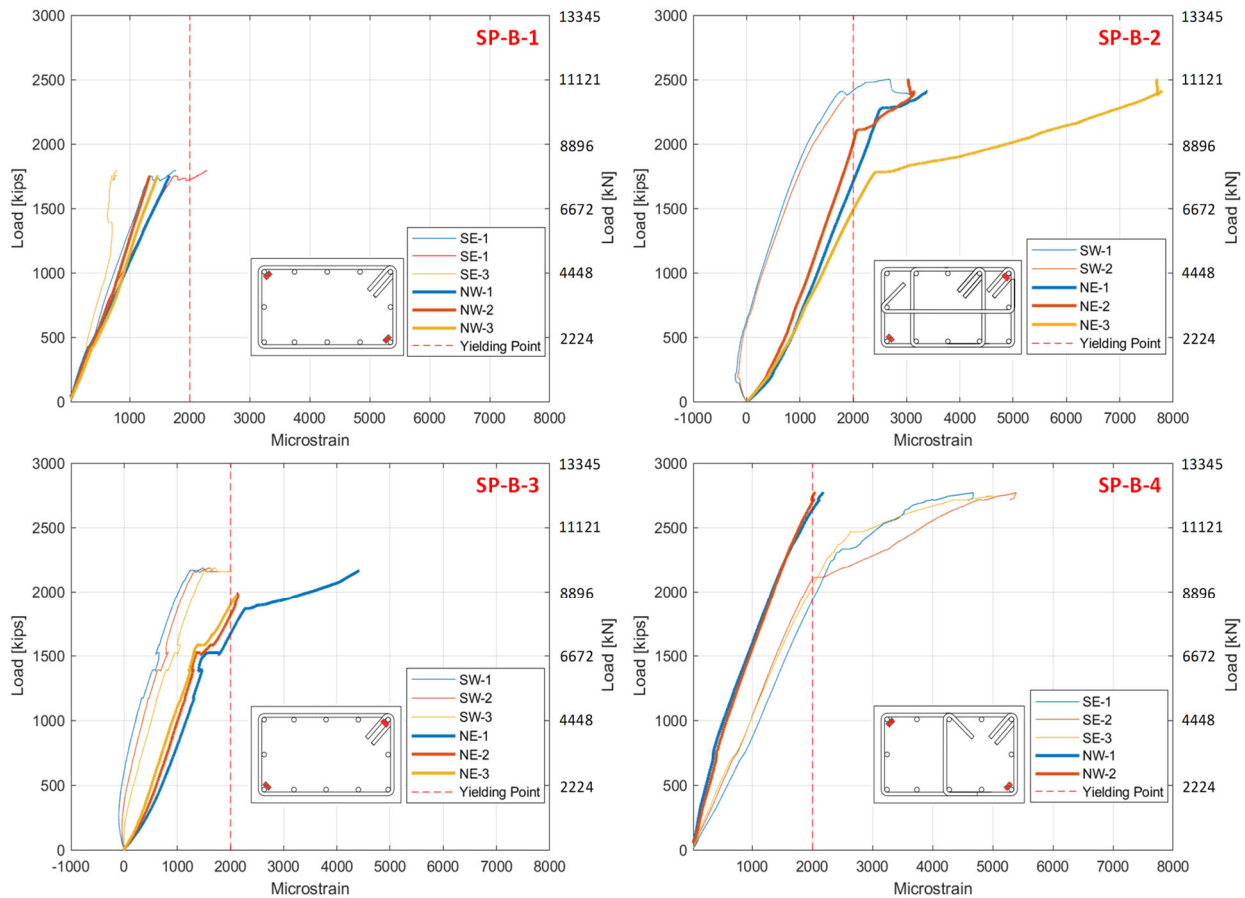


**Figure 4.10** Force versus strain in corner longitudinal bars in Type B rectangular columns

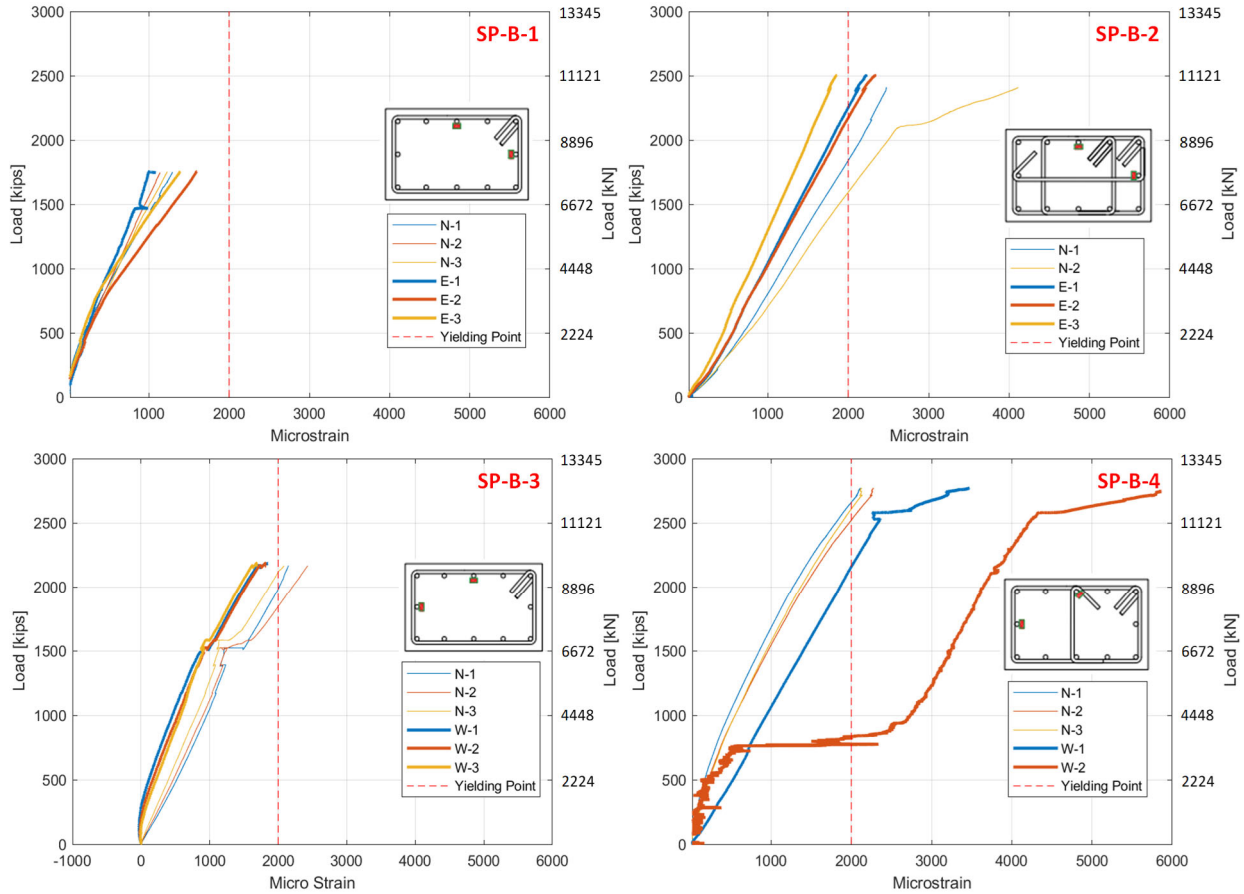


**Figure 4.11** Force versus strain in middle longitudinal bars in Type B rectangular columns

Figures 4.10 through 4.12 show that columns SP-B-2, SP-B-3, and SP-B-4 had slightly more eccentricity than SP-B-1. The force-strain graphs of the longitudinal reinforcement confirm that one side of the columns had suffered more loading than the portion of the column on the opposite side. For the strain captured on transverse rebars, the deviation of the curves at the beginning of the loading, as shown in Figure 4.12, also implies that one of the column's sides was loaded more than the other side. According to Figure 4.12, only SP-B-1 had yielding transverse reinforcement. In every column, at least one of the longitudinal bars yielded before the crushing of concrete. However, none of the transverse reinforcement yielded in SP-B-2, SP-B-3, and SP-B-4, implying that the transverse reinforcement was not fully engaged in these specimens due to the buckling effect of the longitudinal rebars.

Similar to Type A results, the values and percentage of load relative to failure at the onset of the different longitudinal rebars yielding were noted and summarized in Table 4-4.

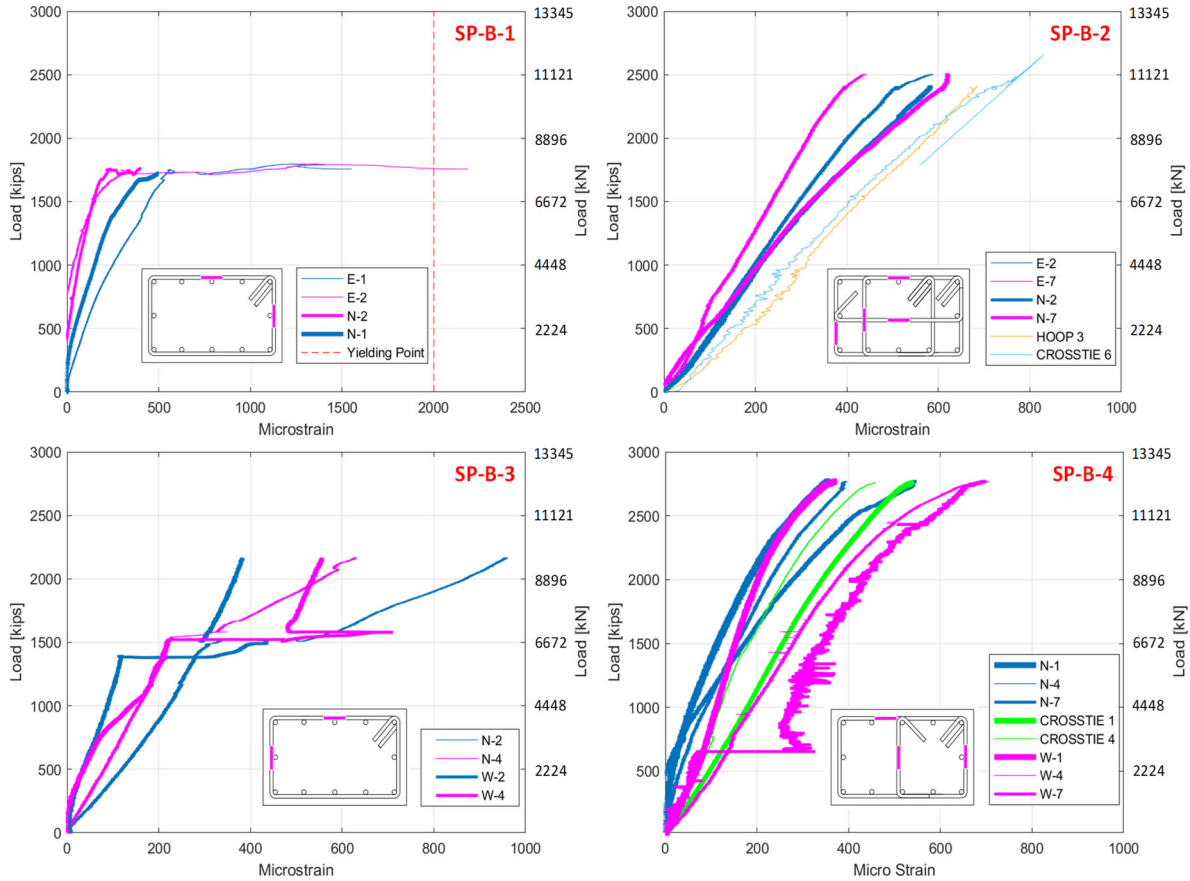


**Figure 4.12** Force versus strain of the transverse bars in columns

**Table 4-4** The yielding strain of the longitudinal bars in Type B columns

Column ID			SP-B-1	SP-B-2	SP-B-3	SP-B-4	
Failure Load [kips]			1,796	2,503	2,186	2,770	
Load at onset of yield	Corner Rebars	NW	kips	1,489	1,676		
			% of failure	59	77		
		SE	kips	2,415			
			% of failure	96			
	NE	kips			2,635		
		% of failure			95		
	SW	kips	1726		1,942		
		% of failure	96		70		
	Middle Rebars	N	kips		1,593	1,846	2,525
			% of failure		64	84	91
		W	kips		2,176		
			% of failure		87		
E		kips				2,159	
		% of failure				78	
Eccentricity Effect?			YES	YES	YES	YES	

#### 4.2.7 Concrete Surface Strain

Selected Type B columns were instrumented with two longitudinal and two lateral concrete gages on the columns' top and bottom south sides. Similar trends captured by the concrete gages were observed in all columns. Therefore, only results from SP-B-1 are shown as an example in this Chapter. Figure 4.13 provides a photograph of the location of the concrete surface strain gages on one of the instrumented columns and close-up views of the different oriented gages. For completeness, selected results captured through concrete gages are also shown in Figure 4.13b to compare local concrete strain against the global strain measured through BR LVDTs as part of the assessment (Figure 4.13c).

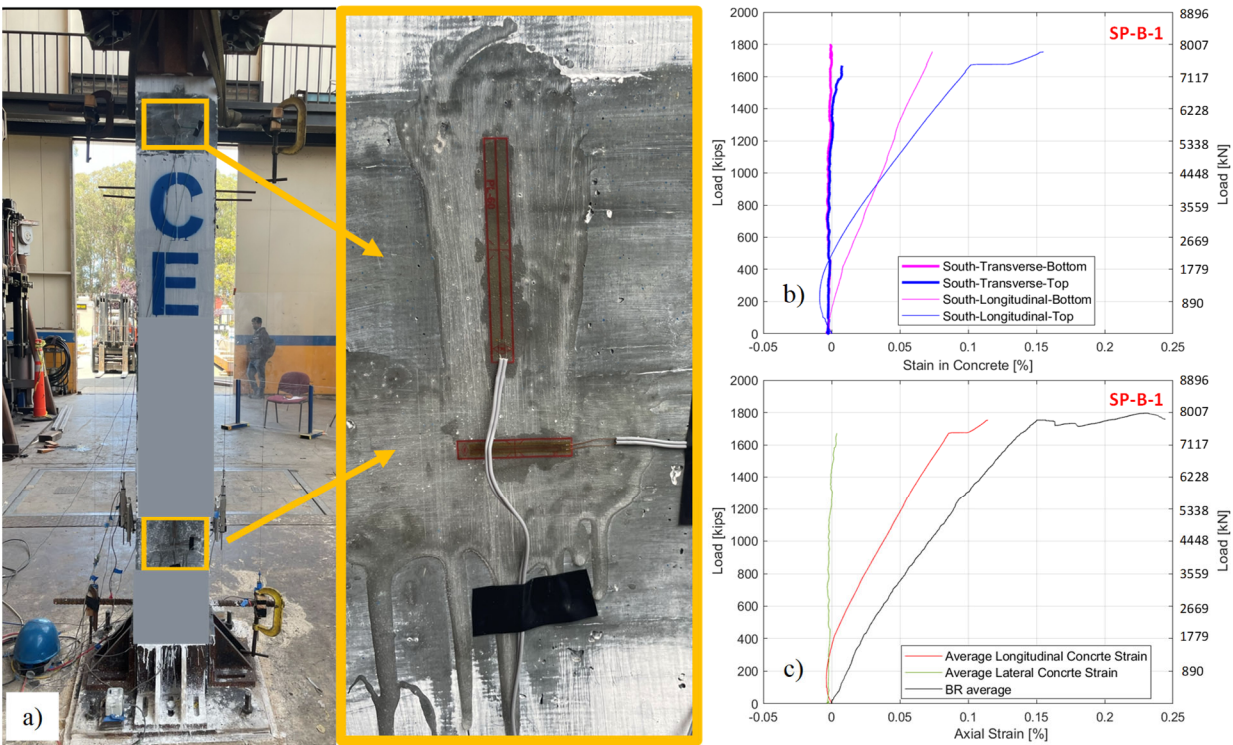


**Figure 4.13** a) concrete gages installed on the top and bottom of the column, b) load versus strain in concrete captured by transverse and longitudinal concrete gages, c) comparison of the average concrete strain captured by longitudinal and lateral concrete gages with the overall axial strain of the column

Figure 4.13 shows a slight deviation between the compressive strain captured by the longitudinal concrete gages and the global strain captured by the LVDTs. The cause of this deviation is that the concrete strain is measured on the south side of the column while the LVDTs capture the global

strain on the column's west side. Both sides experienced different strains due to the minor eccentricity effect.

It was expected for the concrete gages positioned laterally to be in dilation and capture tensile strain or have values close to zero, as is apparent in Figure 4.13b. Furthermore, Figure 4.13b shows that top and bottom concrete gages positioned longitudinally captured tensile strain at the test's beginning and later prolonged into the compression behavior. This is yet another evidence of the eccentricity effects mentioned before.

### 4.3 Type C Columns

Similar to Type A columns, all five columns of Type C UHPC had square cross-sections, as noted and explained previously in Chapter 2. The variables in Type C columns included the transverse reinforcement (spacing and tie configuration), steel fiber ratio (1% and 2%), and steel fiber type (manufactured and recycled). In four columns, manufactured steel fibers were used, i.e. SP-C-1, SP-C-2, and SP-C-3 which used 2%, and SP-C-4 that used only 1%, all by volume. For SP-C-5, recycled tires steel fibers and wires were incorporated using the same weight of manufactured steel fibers of equivalent 2% by volume.

#### 4.3.1 Summary of Key Results

Per the properly reinforced detailing explained earlier, SP-C-1, SP-C-2, and SP-C-3 were considered ACI compliant columns. In addition to the transverse reinforcement with the 3 in (76.2 mm) of spacing, SP-3 and SP-4 had octagonal hoops. While SP-C-4 had only 1%, all other columns had 2% steel fibers by volume. Furthermore, SP-C-5 was the only column that incorporated recycled tire fibers instead of traditional manufactured steel fibers. The weight of recycled tire fibers was the same as the weight of 2% manufactured steel fibers by volume.

Like previous columns, all Type C columns were instrumented with six LVDTs on the north and south sides, while two string pots were positioned on the west and east sides, the same as for the Type A columns. All columns were tested monotonically under concentric axial load through failure, and a summary of the obtained key test results is shown in Table 4-5. The table provides the maximum axial load capacity, strain at peak force, and estimated stiffness for all five columns; which all are inferred and discussed from detailed test results provided in following subsections.

**Table 4-5** Summary of key test results of all five Type C columns

Column ID	Cross-Section Area, in <sup>2</sup> (cm <sup>2</sup> )	Maximum Axial Force, kips (kN)	Strain at Peak	Stiffness, kip/in (kN/mm)
SP-C-1	153.4 (990)	2,136 (9,501)	0.0034	7,727 (1,353)
SP-C-2	147.0 (948)	1,624 (7,224)	0.0035	4,945 (866)
SP-C-3	152.1 (981)	2,316 (10,302)	0.0045	6,465 (1,132)
SP-C-4	157.9 (1,019)	2,095 (9,319)	0.0039	6,684 (1,171)
SP-C-5	149.5 (965)	1,743 (7,753)	0.0039	4,721 (827)

4.3.2 *Damage Progression*

Type C columns' modes of failure and damage photographs after testing and failure are presented in Figure 4.14. All the columns were subjected to axial concentric loading up to the complete loss of the columns' axial capacity as mentioned before. During the loading process, it was observed that columns had some minor crushing of concrete at the top and the bottom. These crushing signs, like previous Type A and B columns, were due to imperfections during the construction, where some longitudinal rebars were positioned and shifted at the ends leading to formwork adjustments that in turn, led to top and bottom ends that were not perfectly parallel. These imperfections led to minor eccentricity effects, which could be observed in the load versus strain graphs that are shown and discussed later.



Figure 4.14 Mode of failure and damage pictures of the five tested Type C columns

The first major damage was the spalling of the cover concrete, visually noticeable by the vertical splitting of the concrete and the slight reduction in load resistance. Due to the high compressive force, longitudinal bars yielded and some have experienced local buckling in between the stirrups

as observed later after failure. Due to the buckling effects of the longitudinal bars at failure, transverse reinforcement was experiencing high tensile forces, and at the end of the testing, some of the transverse bars fractured mostly at the top of the columns. Therefore, most of the columns had a major crack opening starting from the top.

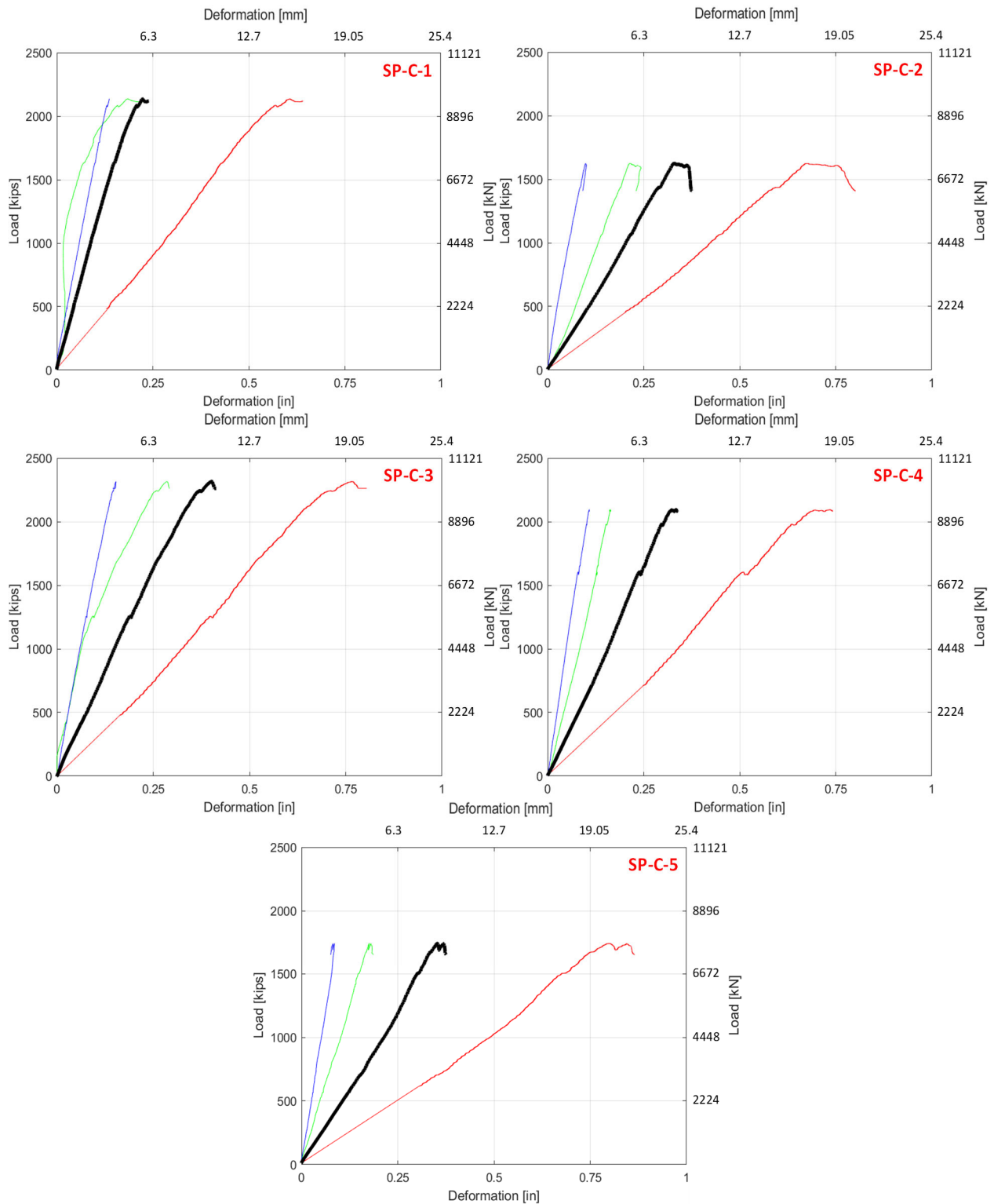
#### *4.3.3 Force versus Deformation Relationships*

Figure 4.15 shows the force versus axial deformation relationships as obtained from the different BR, SR, and SP measurement sets for all Type C columns. The overall average curves from all measurement sets combined is also shown in the figure. Among all three types of UHPC columns, Type C columns have the lowest stiffness and a great variety among the stiffness values (see Figure 4.15 for visual of the curve slopes and Table 4-5 for the estimated and reported stiffness values). As could be noticed from Chapter 3, the Type C UHPC mixture has, in general, a lower modulus of elasticity when compared to the other two types of UHPC. Besides construction errors, the usage of locally available sand and cement can be a reason for a small modulus of elasticity and stiffness values.

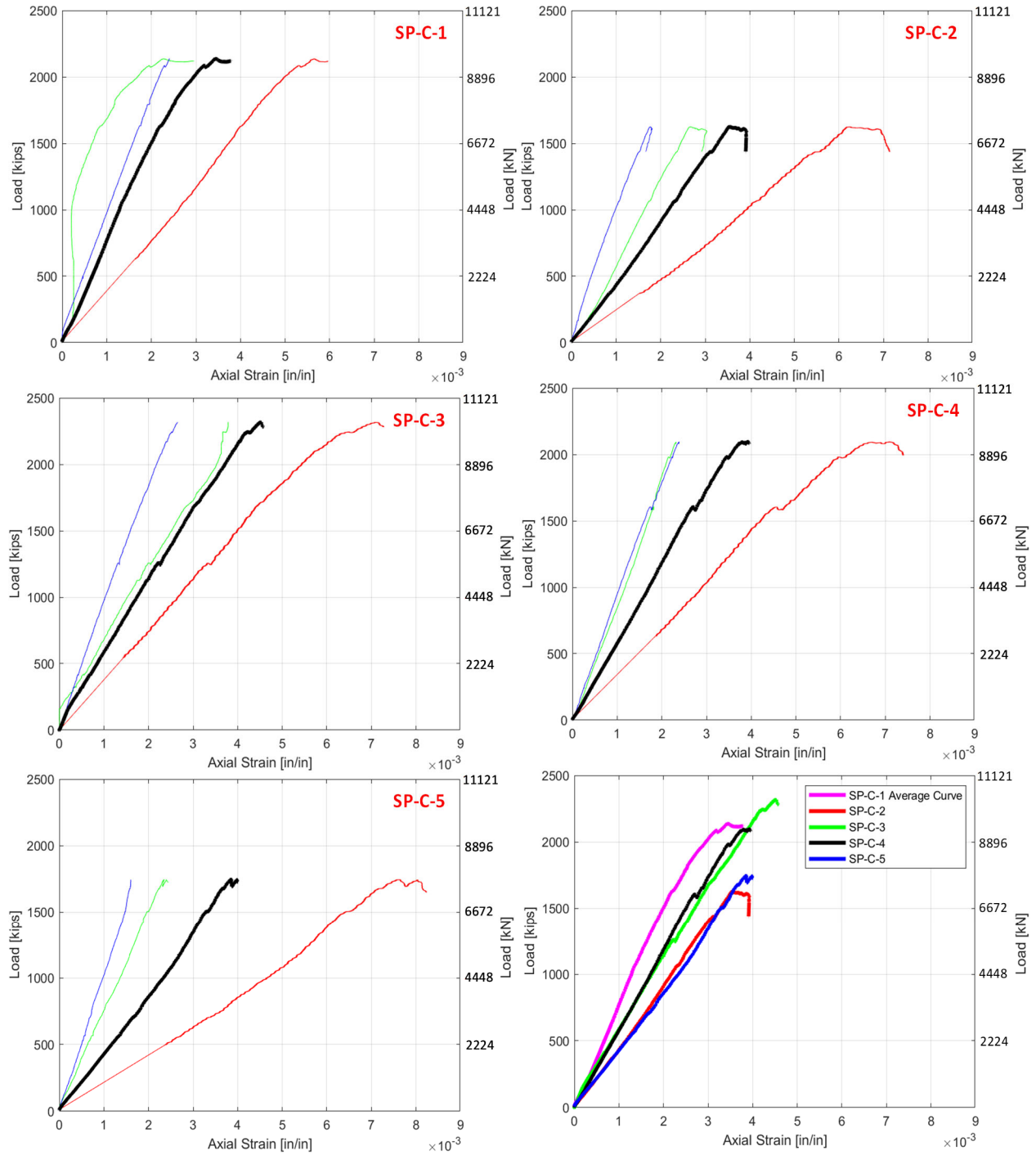
#### *4.3.4 Force versus Axial Strain Relationships*

Figure 4.16 shows force versus axial strain for each column, and the last subplot in that Figure 4.16 present the overall average curves for Type C columns' comparison. Type C columns have higher strain capacities when compared to the other two types of UHPC. SP-C-3 had the highest observed strain capacity, which was expected due to the highest percentage of confinement. SP-C-4 exhibited a little lower strain capacity when compared to the SP-C-3, which can result from a two times lower percentage of the internal confinement-steel fibers.

On the other hand, specimens SP-C-1 and SP-C-2 exhibited similar strain capacities even though the axial load capacity was much lower for the SP-C-2. Later, the reinforcement strains are shown and confirm the eccentricity effects which were found to be most pronounced in SP-C-2 when compared to the other four columns.



**Figure 4.15** Average force versus deformation relationships for all Type C columns using different BR, SR, and SP measurement sets



**Figure 4.16** Force versus axial strain for all five Type C columns and comparisons of overall average curves for five columns together

Furthermore, high strain capacity was observed in the performance of SP-C-5, which contained recycled tire fiber. According to Wang et al. (2000), specimens on a material level containing recycled fibers exhibited similar performance compared to specimens containing steel fibers. The

same case can be observed in this research study. However, due to the high eccentricity and low performance of SP-C-2, it is difficult to compare the performances of SP-C-2 and SP-C-5.

It is worth noting that SP-C-1 outperformed all other Type C columns in terms of axial load capacity. This might be a consequence of using 8 #5 ( $\phi 16$ ) longitudinal bars instead of 12 #4 ( $\phi 13$ ). Rebars with a smaller diameter size have lower critical load capacity. Therefore, they might have a buckling effect much sooner than rebars with a larger diameter leading to premature failure. Even though the longitudinal reinforcement ratios of 8 #5 ( $\phi 16$ ) and 12 #4 ( $\phi 13$ ) have similar values, the performance of individual bars is lower in the case of #4 ( $\phi 13$ ) bars when compared to #5 ( $\phi 16$ ) bars for the same provided transverse reinforcement spacing.

#### 4.3.5 Longitudinal and Transverse Reinforcement Strains

The strain values recorded on the longitudinal and transverse rebars show that all columns have eccentricity. Figures 4.17 through 4.19 show, like before, the force versus longitudinal and transverse reinforcement strain at various locations and levels along height for the different Type C columns. Figures 4.17 and 4.19 confirm that one side of the column suffered more loading than the portion of the column on the opposite side. Also, same as before, the load values and the ratio of such load values to the failure loads at the onset of longitudinal rebar yielding are reported in Table 4-6. The values and percentages in the table also show that longitudinal bars did not yield at the same time due to eccentricity. The figures and table all suggest that SP-C-2 exhibited the highest eccentricity when the strains at opposite sides are compared.

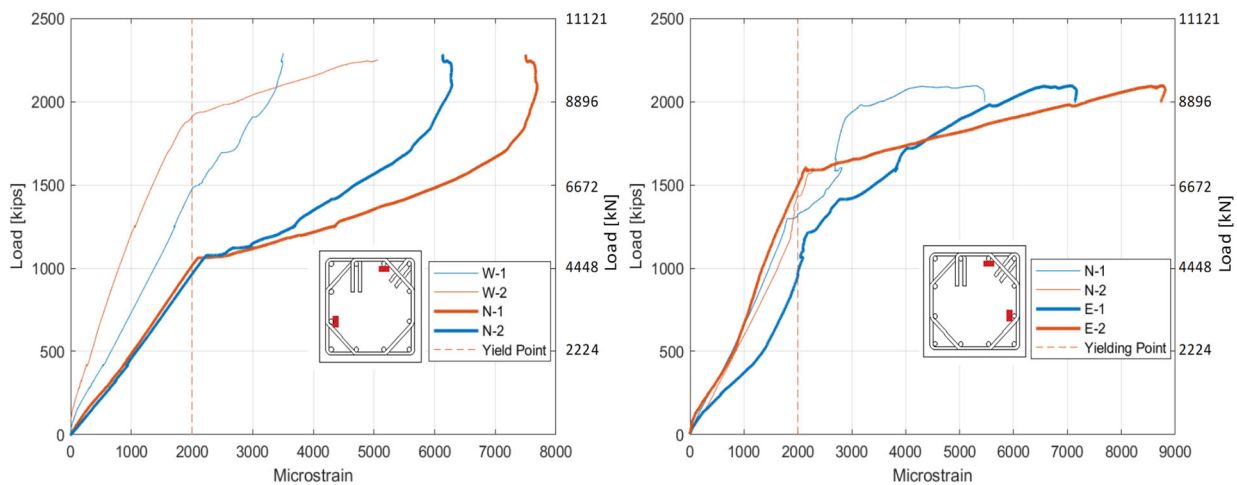


**Figure 4.17** Force versus strain of the middle longitudinal bars in selected Type C columns

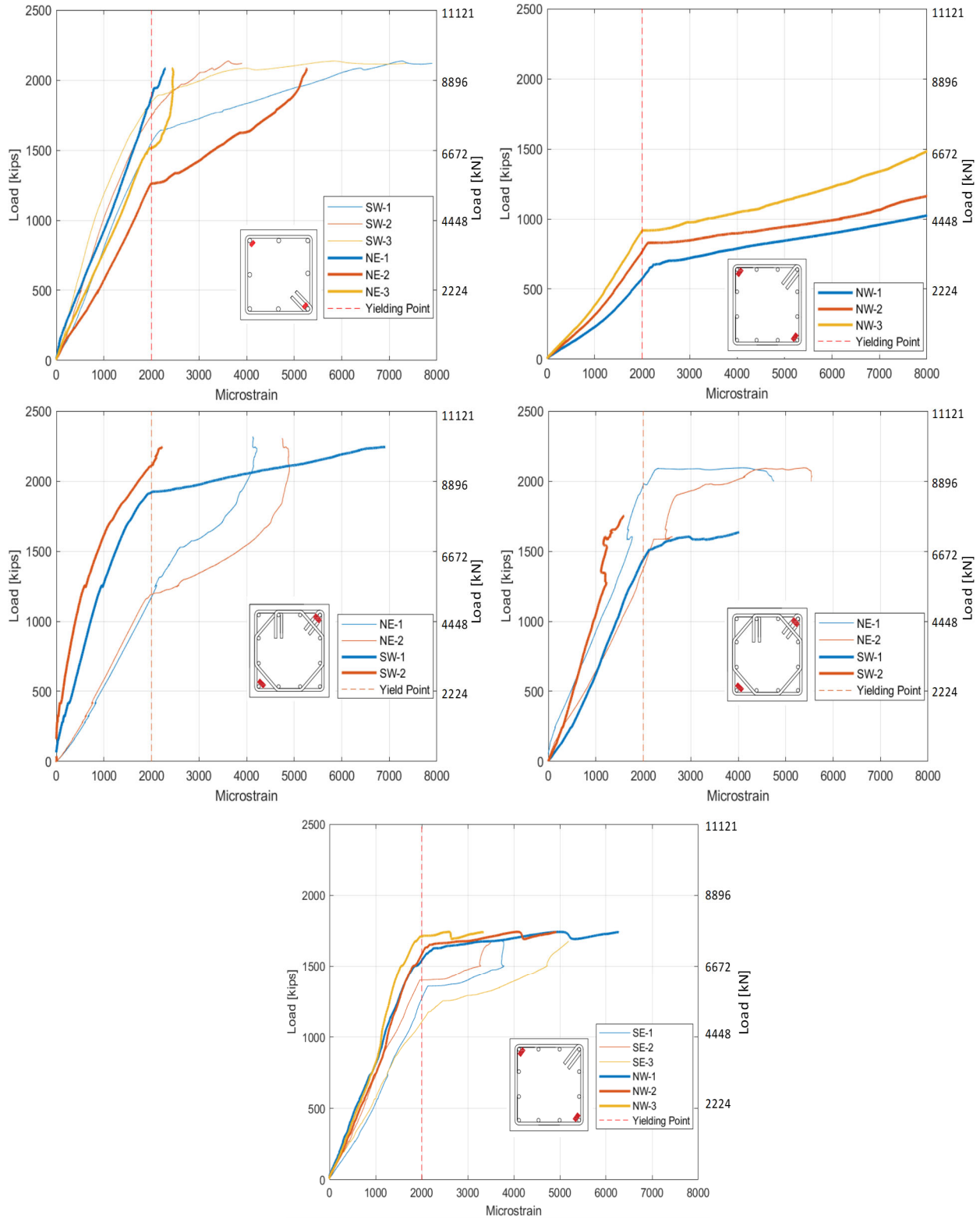


**Figure 4.18** Force versus strain of the corner longitudinal bars in all Type C columns

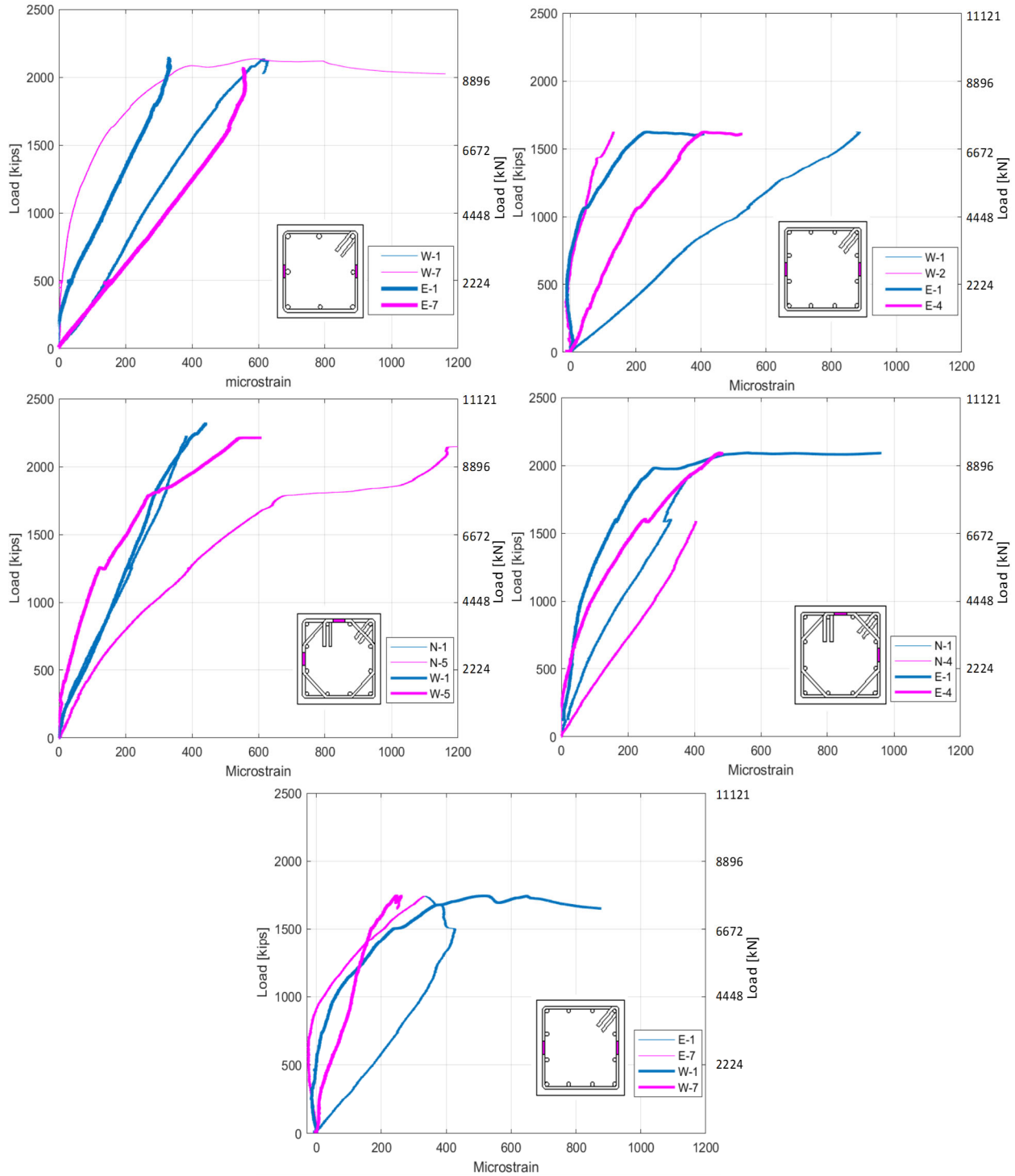


**Figure 4.19** Force versus strain of the transverse reinforcement at different levels along the height in the five Type C columns

Even though strain on the longitudinal reinforcement are captured for the north-west side, the strain gages located on south-east side failed to provide and kind of data. Therefore, the relationship of

the sides can be observed showing a clear deviation of the strain captured on the transverse reinforcement on two opposite sides.

**Table 4-6** The yielding strain of the longitudinal bars in Type C columns

Column ID			SP-C-1	SP-C-2	SP-C-3	SP-C-4	SP-C-4
Failure Load [kips]			2136	1624	2316	2095	1743
Load at onset of yield	Corner Rebars	NW	kips		580.26		1540
			% of failure		36		88
		SE	kips		-		1105
			% of failure		-		63
		NE	kips	1261		119	1376
			% of failure	59		52	66
	SW	kips	1554		1919	1437	
		% of failure	73		83	69	
	Middle Rebars	N	kips			955	1374
			% of failure			41	66
		W	kips			1471	
			% of failure			64	
E		kips				953	
		% of failure				45	
Eccentricity Effect?			YES	YES	YES	YES	YES

## 5 AXIAL LOAD DESIGN AND DETAILING

In this chapter, the actual obtained axial load capacity of the different tested original columns, i.e. four Type A columns, four Type B columns, and five Type C columns, along with the additional columns mentioned before in details in Chapter 2 (Table 2-3), i.e. one Type A column, two Type B columns, and four Type C columns, are all used to assess UHPC columns design and detailing. First, the  $f'_c$  reduction factor, sometimes referred to as size effect, is evaluated and back calculated for UHPC columns using data from 11 ACI compliant columns that are selected from the total of 20 original and additional columns. Next, the design capacity is calculated and compared to actual obtained capacity from testing to obtain a factor of safety that can be used to indirectly assess the transverse reinforcement detailing viability. For the design capacity estimation, accidental eccentricity effects are considered as per ACI provisions. This is needed for accurate assessment giving all the accidental eccentricity cases observed during the actual experimental program and carefully demonstrated in Chapter 4 as part of columns behavior and reinforcement strain discussions.

### 5.1 Calculation of Axial Load Capacity Reduction Factor

For normal strength and conventional concrete columns, the ACI 318 provides Equation 5-1 for estimating a nominal axial strength of axially loaded member, which incorporates some sort of  $f'_c$  reduction factor of 0.85 that we refer to as  $\alpha$  for the sake of this discussion. The equation also uses concrete cylinder's nominal strength ( $f'_c$ ), gross cross-section area of the column ( $A_g$ ), longitudinal reinforcement total area ( $A_{st}$ ), and nominal reinforcing steel yielding stress ( $f_y$ ).

$$P_o = \alpha f'_{c,nominal} (A_g - A_{st}) + f_{y,nominal} A_{st} \quad (5-1)$$

To account for the accidental eccentricity, according to ACI 318-19, the design axial strength should be equivalent to the nominal axial strength reduced by the factor of 0.80 for ties and 0.85 for spirals as presented in Equations 5-2 and 5-3, respectively. Equations 5-2 and 5-3 also incorporate the strength reduction  $\phi$  factor, which is 0.65 for ties and 0.75 for spirals, and as such, we herein refer to the final calculated value using these equations as  $P_{Design}$ .

$$P_{Design} = \phi P_{n,max} = \phi 0.80 \alpha f'_c (A_g - A_{st}) + f_y A_{st} \quad (\text{for ties}) \quad (5-2)$$

$$P_{Design} = \phi P_{n,max} = \phi 0.85 \alpha f'_c (A_g - A_{st}) + f_y A_{st} \quad (\text{for spirals}) \quad (5-3)$$

As previously mentioned, a total of seven additional columns are used in this research study to compliment the 13 original columns presented in Chapter 4 to support the discussion in this chapter. Among the total 20 columns, 11 are considered ACI compliant from a transverse reinforcement requirements and detailing point of view. The actual capacity from testing of such 11 columns were used to estimate or back calculate the  $\alpha$  factor if it were to be used for nominal capacity calculations as shown in Table 5-1.

While the  $\alpha$  is usually used in the design stage where actual material properties are not available, it makes more sense to use nominal material properties in this exercise in our attempt of determining good estimates for  $\alpha$ . Also, the actual material properties reported in Chapter 3 for the various UHPC types used in this study show some inconsistency for the 28-day strength values because of opting for actual site conditions curing as opposed to standard curing. The varying and changing weather and temperature through the course of the experimental program and columns fabrication led to some deviation of cylinders strength from the nominal strength values provided by the manufacturers. Therefore, only nominal UHPC strength values provided by manufacturers are used in this part of the study, which are 20 ksi (~138 MPa) for UHPC Types A and C and 22 ksi (~152 MPa) for Type B.

As explained earlier, columns can be divided into two groups which are considering ACI compliant columns and non-ACI compliant columns. In this case, the properly confined columns are: SP-A-1, SP-A-2, SP-B-2, SP-B-4, SP-C-1, and SP-C-3 from the original set of this study, and SP-B-5, SP-C-6, SP-C-7, SP-C-8, and SP-C-9 from the additional set. It is also noted that SP-C-2 is ACI compliant. However, due to the high eccentricity effect observed for SP-C-2, its structural performance is considered not accurately representative, and therefore, its capacity was excluded from the  $\alpha$  factor calculation presented in Table 5-1.

According to Table 5-1, the average value for the estimated axial load design reduction factor, i.e.  $\alpha$ , is found to be 0.74, which agrees with the value of 0.75 found and proposed by Aboukifa and Moustafa (2022) in a preceding ACI-funded project. Using the data from previous projects along with data from this study and results, a value of 0.75 is then recommended to be used for future UHPC axial strength capacity estimation.

**Table 5-1** Axial load design reduction ( $\alpha$ ) factor estimation using ACI-compliant columns

Column ID		$f'_c$ nominal	$P_{max}$ [kips]	$A_c$ [in <sup>2</sup> ]	$A_s$ [in <sup>2</sup> ]	$f_y$ [ksi]	estimated $\alpha$
Original columns	SP-A-1	20.0	2504.2	155.9	2.5	60.0	0.77
	SP-A-2	20.0	2388.6	144.8	2.5	60.0	0.79
	SP-B-2	22.0	2503.1	163.4	2.4	60.0	0.67
	SP-B-4	22.0	2769.6	167.9	2.4	60.0	0.72
	SP-C-1	20.0	2136.4	153.4	2.5	60.0	0.66
	SP-C-3	20.0	2315.9	152.1	2.4	60.0	0.73
Additional columns	SP-B-5	22.0	2590.3	148.4	2.5	60.0	0.76
	SP-C-6	20.0	3288.4	201.1	4.4	60.0	0.77
	SP-C-7	20.0	3419.2	201.1	4.4	60.0	0.80
	SP-C-8	20.0	3021.1	201.1	4.4	60.0	0.70
	SP-C-9	20.0	3458.6	201.1	4.4	60.0	0.81
<i>Average</i>							<b>0.74</b>

## 5.2 Effect of Transverse Reinforcement Detailing

In this study, the transverse reinforcement provided for several UHPC columns was deliberately designed and detailed to be non-ACI compliant to investigate whether some of the ACI provisions can be relaxed for UHPC columns. For instance, several columns used wide transverse reinforcement spacing that violates the threshold value for the spacing to longitudinal bar diameter ratio, i.e.  $s/d_b \leq 6$ . Other columns, specially Type B rectangular ones, did not use any cross-ties or internal stirrups and had longitudinal rebars that were not properly laterally constrained as per ACI detailing requirements. The hypothesis here was to determine whether the steel fibers and internal structure of UHPC can provide some self-confinement that could alleviate some of the stringent transverse reinforcement requirements. Overall, the comparative behavior in terms of axial capacity and strain data presented in Chapter 4 prove the above hypothesis wrong. This is because most of non-ACI compliant columns underperformed when compared to compliant ones even though no real or significant benefits or increase in capacities could be tied to proper confinement.

To take a second look at the hypothesis above and assess transverse reinforcement detailing effects from a different perspective, the design capacity ( $\phi P_{n,max}$ ) for all 20 columns is recalculated using the confirmed 0.75 value for  $\alpha$  and compared to the actual obtained axial capacity from testing

( $P_{max, test}$ ) to obtain some sort of a factor of safety for design. The results are provided in Table 5-2 for all 20 columns along with identifying whether each column is ACI compliant for transverse reinforcement requirements.

The results in Table 5-2 show an overall average factor of safety of 1.66 which is reasonable and suggests that the calibrated design equation with  $\alpha = 0.75$  and the current various ACI reduction factors for axial members can be used for UHPC axial columns. Moreover, the relatively lower factors of safety can be immediately noticed to be tied to non-ACI compliant transverse reinforcement, which is again confirm the observations made from the behavior and response discussed before and suggests that current ACI detailing requirements should be used in general for UHPC columns without relaxing any specific provisions.

**Table 5-2** Design and actual axial capacity of UHPC columns with varying transverse reinforcement detailing and ACI compliance

UHPC Type and Columns ID		SF Ratio [%]	ACI Compliant?	$P_{max, test}$ [kips]	$\phi P_{n,max}$ [kips]	Factor of Safety = $P_{max} / \phi P_{n,max}$
Type A	SP-A-1	2%	Yes	2504.2	1333.6	1.9
	SP-A-2	2%	Yes	2388.6	1243.0	1.9
	SP-A-3	2%	No	2105.2	1208.3	1.7
	SP-A-4	2%	No	1904.0	1235.3	1.5
	SP-A-5	1%	Yes	2013.4	1299.2	1.5
Type B	SP-B-1	2%	No	1796.3	1518.6	1.2
	SP-B-2	2%	Yes	2503.1	1456.0	1.7
	SP-B-3	2%	No	2185.7	1501.4	1.5
	SP-B-4	2%	Yes	2769.6	1494.9	1.9
	SP-B-5	2%	Yes	2590.3	1329.3	1.9
	SP-B-6	1%	Yes	1623.5	1281.8	1.3
Type C	SP-C-1	2%	Yes	2136.4	1254.5	1.7
	SP-C-2	2%	No	1623.6	1202.7	1.3
	SP-C-3	2%	Yes	2315.9	1242.5	1.9
	SP-C-4	1%	Yes	2094.6	1288.1	1.6
	SP-C-5	2% recyc.	No	1742.9	1222.1	1.4
	SP-C-6	2%	Yes	3288.4	2048.9	1.6
	SP-C-7	2%	Yes	3423.2	2048.9	1.7
	SP-C-8	2%	Yes	3021.1	1671.2	1.8
	SP-C-9	2%	Yes	3458.6	1671.2	2.1
<i>Average</i>					<i>1.66</i>	

## **6 CONCLUDING REMARKS**

### **6.1 Summary**

This study aimed at investigating the experimental structural behavior of 13 UHPC columns that varied in the UHPC mixtures and transverse reinforcement detailing when subjected to axial compressive loading. The study considered three emerging UHPC mixtures that were not commonly used for structural or large research applications before so that the obtained results complement the existing research body that focused on traditional UHPC, and help general the design recommendations provided herein. The mixtures included a UHPC type that uses white cement (UHPC Type A), carbon nanofibers enhanced UHPC (Type B), and semi-proprietary UHPC with local sand and cement (Type C).

In addition to the 13 columns presented in detail in this report, seven more full-scale columns were used in the design and reinforcement detailing assessments. Out of the 20 columns, a total of 16 columns were fabricated at the University of Nevada, Reno and four were fabricated at a precast facility in CA (4 of the additional columns). However, all 20 columns were tested at the University of California, Berkeley PEER Laboratory at the 4000-kip (~18,000 kN) testing machine. The variables considered in the experimental program among the different columns included varying the type of UHPC mixture, transverse and longitudinal reinforcement ratios, cross-section area, percentage of steel fibers, and type of micro confinement.

Moreover, this study evaluated the applicability of ACI 318 equations and procedures for axial UHPC columns capacity prediction and a key factor in the equations has been revised and calibrated. Also, the columns behavior was comparatively assessed to better understand the effect of transverse reinforcement detailing and whether there is room for relaxing some of those detailing provisions for future UHPC columns.

### **6.2 Key Observations and Conclusions**

Several observations and conclusions can be drawn based on the discussed results. The findings from the different components of the conducted experimental study and the relevant ACI 318 provisions assessment on full-scale UHPC columns led to the following conclusions:

- In the process of determining the modulus of elasticity of UHPC cylinders, the region between 10-30% of compressive stress is best to use in order to avoid the initial softening part of the

curve influenced by the loading head adjustment to the specimen and final nonlinear part of the curve when approaching the peak and failure.

- The modulus of elasticity of Type B UHPC as obtained from  $3 \times 6$  in ( $75 \times 150$  mm) cylinders is the highest among all three types of UHPC mixtures, which might be attributed to the carbon nanofiber effect. However, the UHPC Type C cylinders exhibited the lowest modulus of elasticity values, which might be due to the nature of the semi-proprietary UHPC mixture where sand and cement were sourced locally.
- In this study, it is shown that adding higher dosage of accelerator to UHPC can have significant adverse effects on construction quality because accelerator increase mixing heat and cause earlier setting, which reduces the workability and flowability, and in turn, is not suitable for large structural components where several batches are needed. The higher accelerator dosage used for Type B UHPC resulted in honeycombing and later, clear delamination of columns after testing.
- Casting UHPC in very cold weather without proper heat treatment can lead to delayed hydration due to frozen water particles. Some of the companion cylinders that were left to cure next to columns during winter time did not get to even 70% of expected strength at 28 days, and continued to gain strength for several months after construction.
- The orientation of steel fibers may not distress columns significantly, but in the specimens that were already exposed to some construction difficulties as in case of Type B columns, the parallel to flow and column longitudinal axis steel fiber orientation may have caused additional adverse effects on the overall structural behavior of the respective specimens.
- When the structural behavior of the UHPC columns with complying transverse reinforcement spacing to longitudinal bar diameter ratio ( $s/d_b$ ) is compared to non-complying cases, it becomes clear that smaller spacing and compliant  $s/d_b$  values are still necessary for UHPC columns. In other words, the steel fibers and UHPC structure do not provide additional meaningful lateral constraining for rebars nor fully prevent local rebar buckling.
- UHPC columns with 1% steel fibers by volume ratio did not seem to have a favorable comparable structural response as the cases of using the typical 2% ratio. As such, it is

recommended to consider 2% or higher steel fiber ratios for axial UHPC columns even if other structural applications such as deck joints can use only 1% steel fibers ratio.

- The single tested column specimen that used recycled tire steel fibers performed similarly to the column incorporating 2% of virgin manufactured steel fibers, which is very promising and suggests that recycled tire fibers can be a good substitute for manufactured steel fibers to lower the cost and make UHPC mixtures more sustainable when used in future columns. Nevertheless, more research is still needed to fully exploit the potential and limitations of using recycled fibers in structural UHPC applications.
- Over-confining UHPC columns using additional transverse reinforcement beyond what would be typically required by ACI provisions does not necessarily benefit the structural response and axial capacity. In fact, the most confined rectangular column considered in this study was shown to be adversely affected by the excess transverse reinforcement that hindered the smooth flowability and steel fibers dispersion within the column.

### 6.3 Design Recommendations

The main design recommendations and guidance obtained from this study are short and simple yet comprehensive and can be generalized as per the discussions in Chapter 5. Such design and detailing recommendations for axial UHPC columns are summarized again here for completeness.

- For estimating axial design capacity of UHPC columns, the following ACI 318 equations (Equations 6-1 through 6-3) can be used with the proposed modification of using an  $\alpha$  factor of 0.75 as opposed to the current value of 0.85 that is only suitable for conventional and normal strength concrete. Meanwhile, the current accidental eccentricity reduction factors and strength reduction factor ( $\phi$ ) for tied and spiral columns seem to offer reasonable margin of safety and are recommended to continue to use for UHPC columns. Nevertheless, future work and studies are recommended to carry out reliability and statistical analyses if such factors were to be revisited for UHPC.

$$P_o = \alpha f'_{c,nominal} (A_g - A_{st}) + f_{y,nominal} A_{st} \quad (6-1)$$

$$P_{Design} = \phi P_{n,max} = \phi 0.80 \alpha f'_c (A_g - A_{st}) + f_y A_{st} \quad (for\ ties) \quad (6-2)$$

$$P_{Design} = \phi P_{n,max} = \phi 0.85 \alpha f'_c (A_g - A_{st}) + f_y A_{st} \quad (for\ spirals) \quad (6-3)$$

- For transverse reinforcement detailing, current ACI 318 provisions should be used for UHPC columns where the additional benefits from using steel fibers, such as in shear, do not really hold for confinement. For instance, longitudinal rebars in UHPC columns should be laterally constrained at corner or two sides of orthogonal ties every 6 inches or less as per current provisions. Moreover, the steel fibers and internal structure of UHPC do not offer extra lateral buckling support for longitudinal bars in between the stirrups, and accordingly, the typical required  $s/d_b$  limit (i.e.  $s/d_b \leq 6$ ) should be taken into account in UHPC columns.

## REFERENCES

- Abdolpour, H., Niewiadomski, P., & Sadowski, Ł. (2021). Recycling of steel fibres and spent equilibrium catalyst in ultra-high performance concrete: Literature review, Research Gaps, and future development. *Construction and Building Materials*, 309, 125147. <https://doi.org/10.1016/j.conbuildmat.2021.125147>
- Abokifa, M., & Moustafa, M. A. (2021a). Mechanical characterization and material variability effects of emerging non-proprietary UHPC mixes for accelerated bridge construction field joints. *Construction and Building Materials*, 308, 125064.
- Abokifa, M., & Moustafa, M. A. (2021b). Experimental behavior of precast bridge deck systems with non-proprietary UHPC transverse field joints. *Materials*, 14(22), 6964.
- Abokifa, M., & Moustafa, M. A. (2022a). Reinforcement detailing effects on axial behavior of full-scale UHPC columns. *Journal of Building Engineering*, 49, 104064.
- Abokifa, M., & Moustafa, M. A. (2022b). Structural and buckling behavior of full-scale slender UHPC columns. *Engineering Structures*, 255, 113928.
- Berry, M., Snidarich, R., & Wood, C. (2017). *Development of non-proprietary ultra-high performance concrete* (No. FHWA/MT-17-010/8237-001). Montana. Dept. of Transportation. Research Programs.
- Cimesa, M., & Moustafa, M. A. (2022). Experimental characterization and analytical assessment of compressive behavior of carbon nanofibers enhanced UHPC. *Case Studies in Construction Materials*, 17, e01487.
- Cai, H., Xu, L., Chi, Y., Yan, Y., Yu, C., & He, C. (2021). Seismic performance of rectangular ultra-high performance concrete filled steel tube (UHPCFST) columns. *Composite Structures*, 259, 113242.
- Du, J., Meng, W., Khayat, K. H., Bao, Y., Guo, P., Lyu, Z., ... & Wang, H. (2021). New development of ultra-high-performance concrete (UHPC). *Composites Part B: Engineering*, 224, 109220.
- Du, J., Meng, W., Khayat, K. H., Bao, Y., Guo, P., Lyu, Z., ... & Wang, H. (2021). New development of ultra-high-performance concrete (UHPC). *Composites Part B: Engineering*, 224, 109220.

- El-Tawil, S., Alkaysi, M., Naaman, A. E., Hansen, W., & Liu, Z. (2016). *Development, characterization and applications of a non proprietary ultra high performance concrete for highway bridges* (No. RC-1637). Michigan. Dept. of Transportation.
- Graybeal, B. A. (2005). *Characterization of the behavior of ultra-high performance concrete*. University of Maryland, College Park.
- Graybeal, B. A. (2006). *Material property characterization of ultra-high performance concrete* (No. FHWA-HRT-06-103). United States. Federal Highway Administration. Office of Infrastructure Research and Development.
- Graybeal, B. A. (2013). *Development of non-proprietary ultra-high performance concrete for use in the highway bridge sector: TechBrief* (No. FHWA-HRT-13-100). United States. Federal Highway Administration.
- Hamad, B. S. (1995). Investigations of chemical and physical properties of white cement concrete. *Advanced Cement Based Materials*, 2(4), 161-167.
- Heshe G, Nielsen CV (1992). Behaviour in compression, triaxial stress state and short columns. Report EU264-Compressit Aalborg Portland, Aalborg, 51p.
- Heshe G, Nielsen CV (1992). Behaviour in compression, triaxial stress state and short columns. Report EU264-Compressit Aalborg Portland, Aalborg, 51p.
- High-performance concrete (No. FHWA/MT-17-010/8237-001). Montana. Dept. of Transportation. Research Programs.
- Hosinie, M. M., Aoude, H., Cook, W. D., & Mitchell, D. (2015). Behavior of ultra-high performance fiber reinforced concrete columns under pure axial loading. *Engineering Structures*, 99, 388-401.
- MORESOVA, Karterina, and Frantisek SKVARA. "White cement: Properties, manufacture, prospects." *Ceramics (Praha)* 45, no. 4 (2001): 158-163.
- Liew, K. M., & Akbar, A. (2020). The recent progress of recycled steel fiber reinforced concrete. *Construction and Building Materials*, 232, 117232. <https://doi.org/10.1016/j.conbuildmat.2019.117232>

- Meng, W., & Khayat, K. H. (2018). Effect of graphite nanoplatelets and carbon nanofibers on rheology, hydration, shrinkage, mechanical properties, and microstructure of UHPC. *Cement and Concrete Research*, 105, 64-71.
- Naeimi, N., & Moustafa, M. A. (2021). Compressive behavior and stress–strain relationships of confined and unconfined UHPC. *Construction and Building Materials*, 272, 121844.
- Sbia, L. A., Peyvandi, A., Soroushian, P., Lu, J., & Balachandra, A. M. (2014). Enhancement of Ultrahigh Performance Concrete Material Properties with Carbon Nanofiber. *Advances in Civil Engineering*.
- Yang, J., Peng, G.-F., Shui, G.-S., & Zhang, G. (2019). Mechanical properties and anti-spalling behavior of ultra-high performance concrete with recycled and industrial steel fibers. *Materials*, 12(5), 783. <https://doi.org/10.3390/ma12050783>
- Yoo, D. Y., Oh, T., & Banthia, N. (2022). Nanomaterials in ultra-high-performance concrete (UHPC)—A review. *Cement and Concrete Composites*, 104730.